ORNL/TM-2023/2992

Oak Ridge National Laboratory
Report on initial development of a database of nuclear graphite characteristics based on microstructural characterization

J. David Arregui-Mena
Nidia C. Gallego

July 2023

ORNL IS MANAGED BY UT-BATTELLE LLC FOR THE US DEPARTMENT OF ENERGY

DOCUMENT AVAILABILITY

Reports produced after January 1, 1996, are generally available free via OSTI.GOV.

Website www.osti.gov

Reports produced before January 1, 1996, may be purchased by members of the public from the following source:

National Technical Information Service
5285 Port Royal Road
Springfield, VA 22161
Telephone 703-605-6000 (1-800-553-6847)
TDD 703-487-4639
Fax 703-605-6900
E-mail info@ntis.gov
Website http://classic.ntis.gov/

Reports are available to US Department of Energy (DOE) employees, DOE contractors, Energy Technology Data Exchange representatives, and International Nuclear Information System representatives from the following source:

Office of Scientific and Technical Information
PO Box 62
Oak Ridge, TN 37831
Telephone 865-576-8401
Fax 865-576-5728
E-mail reports@osti.gov
Website https://www.osti.gov/

This report was prepared as an account of work sponsored by an agency of the United States Government. Neither the United States Government nor any agency thereof, nor any of their employees, makes any warranty, express or implied, or assumes any legal liability or responsibility for the accuracy, completeness, or usefulness of any information, apparatus, product, or process disclosed, or represents that its use would not infringe privately owned rights. Reference herein to any specific commercial product, process, or service by trade name, trademark, manufacturer, or otherwise, does not necessarily constitute or imply its endorsement, recommendation, or favoring by the United States Government or any agency thereof. The views and opinions of authors expressed herein do not necessarily state or reflect those of the United States Government or any agency thereof.

ORNL/TM-2023/2992

Materials Science and Technology Division

REPORT ON INITIAL DEVELOPMENT OF A DATABASE OF NUCLEAR GRAPHITE CHARACTERISTICS BASED ON MICROSTRUCTURAL CHARACTERIZATION

J. David Arregui-Mena
Nidia C. Gallego

July 2023

Prepared by
OAK RIDGE NATIONAL LABORATORY
Oak Ridge, TN 37831
managed by
UT-BATTELLE LLC
for the
US DEPARTMENT OF ENERGY
under contract DE-AC05-00OR22725

CONTENTS

LIST OF FIGURES

LIST OF TABLES

ABSTRACT

This report outlines the current and ongoing efforts to produce a comprehensive library of microstructures of nuclear graphite and carbon-based materials that are candidate materials for nuclear applications in the United States. This library contains extensive characterizations of unirradiated graphite materials, a guide to some of the techniques used to characterize graphite, a compendium of characterization data of neutron-irradiated or oxidized material, and a compendium of microstructural information of carbon-based materials. These characterization efforts are being conducted at various length scales to understand these complex materials' local structure and property relationships. Achieving this goal requires further developing or adapting advanced characterization techniques that capture graphite's most relevant characteristics.

Some of the general objectives of this project are to aid with the material selection, licensing, management, and core assessments of a graphite core by documenting the unirradiated microstructure of relevant grades or by characterizing the evolution of the microstructure under the reactor environment. Moreover, this project aims to provide additional information, guidelines for characterizing graphite, and a protocol to assess a nuclear graphite grade.

This report also summarizes some of the initial results and some of the techniques commonly used to characterize nuclear graphite.

1. INTRODUCTION

To support the commercialization of power generation via graphite-moderated reactors in the United States, it is essential to evaluate and classify materials and systems that can ensure the long-term reliability of the next generation of nuclear power plants. The US Department of Energy's Oak Ridge National Laboratory (ORNL) nuclear graphite group is constructing a library of microstructures that will help identify the key phases, characteristics, techniques, and graphite materials for advanced non-light-water reactors, specifically those in the GEN IV category.

Graphite is a critical moderator and structural material for Generation IV advanced reactors, including the Very High-Temperature Reactor (VHTR) [1] and various molten salt reactor (MSR) designs [2]. Unlike metals used in conventional power-generating reactors, graphite is a complex material formed by filler and binder phases. Graphite's properties depend on the distribution, characteristics, and raw materials of the filler and binder phases [3]. To confidently predict and inspect the long-term performance in either gas-cooled or molten salt environments, the nuclear industry requires a deeper understanding of the fundamental relationships between processing, structure, and properties of graphites as well as the availability, sourcing, and performance variations of different graphite types.

The development and operation of graphite-moderated reactors pose a unique material challenge for the US nuclear industry. Since the closure of the Fort St. Vrain power reactor in 1989, graphite-moderated reactors have not operated in the United States, resulting in a significant loss of operational knowledge regarding graphite in reactors. This knowledge gap, along with limited public data and expertise, necessitates extensive microstructural characterization that expands understanding of the neutron irradiation effects, oxidation, and fracture behavior in modern graphite materials. To effectively and reliably employ graphite in advanced reactors, the United States must create a baseline microstructural analysis that expands the current data. Identifying critical knowledge gaps such as neutron irradiation effects or oxidation, graphite material variability, and describing the limitations and advantages of various microscopy and analytical techniques used to characterize a nuclear graphite core will advance the deployment and aid with the regulatory frameworks and licensing in the United States. Moreover, the library of microstructures will provide a robust collection of as-received, oxidized, and neutron-irradiated microstructures that can be used to understand the evolution of graphite damage in a reactor environment and thus help monitor a graphite core.

This report comprises five sections: a general description of nuclear graphite, a guideline to understand the different techniques commonly used to study graphite, a baseline library of microstructures, a library of defects caused by oxidation and/or neutron irradiation, and brief library of carbon materials used in the nuclear industry. These thrusts will help inform the industry about the characteristics of nuclear graphite and other carbon-based materials, inform surveillance campaigns of reactor cores, and enable the modeling and validation of stress analysis and fracture mechanics models. In particular, data about graphite's microstructure can be used as inputs to study the performance of particular graphite grades [4, 5]. This library will support the following efforts:

- *Design and selection of nuclear grades*—The design and selection of graphite materials and components depend on the application and conditions generated by the reactor design. The microstructure characterization of nuclear grades will improve the fundamental understanding of aging processes and cracking generated by the reactor environment. This research will also improve guidance regarding the microstructural characterization of graphite to ensure consistent the materials and support any judgments on the adequacy of the graphite materials.

- *Manufacture and commissioning*—Nuclear graphite is a heterogeneous material that can contain multiple flaws generated during manufacturing. This research will help develop protocols to identify differences between grades, intragrade variations, and defects found in graphite at multiple length scales. This research will examine different ways to quantify the uncertainty related to graphite production and microstructural heterogeneity in graphite.

- *Defect monitoring*—Even though the design and modeling formulate multiple safety case scenarios, it is necessary to establish the damage tolerance and safety margins for a reactor core. These limits might be directly assessed from reactor monitoring inspections. However, limited microstructural data can be used to compare or quantify the bounds for operating a graphite-moderated nuclear reactor. This project will obtain and characterize materials to help establish the bounds for safe operation.

- *Assessments of core aging caused by the reactor environment, fuel refueling, or oxidation*—Nuclear graphite components are subjected to cooling and thermal shock during refueling operations, and neutron irradiation induces defects and oxidation. This research will mimic some of these conditions to observe how the microstructure evolves as a function of degradation mechanisms. Moreover, this project is investigating some features in graphite that can be used as forensic fingerprints that reveal the history of dimensional change in a graphite component. Materials Test Reactor (MTR) irradiation campaign experiments are normally used as input information for material properties into design calculations. However, the microstructural information of these samples is not normally recorded. Linking the microstructural evolution with mechanical properties will enable better core behavior predictions.

- *Sampling and testing of core components*—In some cases, the United Kingdom has commissioned sampling trepanned graphite cores from moderator bricks. These cores are used to elucidate the state and health of the brick and overall reactor core. Adopting this practice in the United States would require then a baseline of irradiated material characteristics that could be compared with the trepanned cores. This research involves documenting some defects generated by the reactor core so they can be compared against irradiated material.

This report establishes part of the library's objectives, describes the general aspects of graphite, and includes the first preliminary baseline of microstructural characterization and a literature review of some techniques commonly used to characterize nuclear graphite.

2. NUCLEAR GRAPHITE

Graphite was the moderator material of the first nuclear reactors and is used or being proposed for use in the current fleet of British advanced gas-cooled reactors (AGR) and Generation IV concepts such as the VHTRs and MSRs in the United States. Neutron irradiation causes volumetric and mechanical property changes that promote the cracking of graphite components. The failure of multiple graphite components may alter the current circulation of coolant or refueling operations, making the graphite core a lifetime-limiting component of all AGR power stations and in some VHTR and MSR designs. Several efforts have been undertaken to assess the structural integrity of graphite at a macroscopic level, such as project Blackstone in the United Kingdom and the Advanced Graphite Creep (AGC) program [6] in the United States. Nevertheless, some of the microstructural characteristics, irradiation effects, and irradiation creep effects on the microstructure of graphite remain unknown. A selection of as-received and irradiated nuclear graphite samples obtained from the AGC campaign will be used to understand the overall microstructure of candidate graphite grades and some aspects of irradiation effects.

Several key requirements must be met to ensure the reliable operation of a graphite reactor core, including maintaining structural integrity, facilitating fueling operations, and ensuring the continuous circulation of coolant under both normal and fault conditions. To achieve these crucial functions, conducting microstructural characterization is imperative and enables a comprehensive understanding and prediction of graphite degradation mechanisms within the reactor environment.

2.1 MANUFACTURE OF GRAPHITE

To understand the resulting graphite's microstructure its influence on graphite's mechanical properties, it is necessary to describe the manufacturing processes of this material. Graphite can be considered a composite because it is a mixture of multiple carbon-rich materials that form a porous polycrystalline material. Most of the general steps to manufacture graphite are described below and are illustrated in Figure 1.

1. Various coke sources can serve as raw materials for nuclear graphite. These materials include petroleum coke, pitch coke, and naturally occurring sources such as derivatives of Gilsonite used in UK AGR graphite components. The shape of this raw constituent can influence the mechanical isotropy or anisotropy of the resulting graphite. For example, the combination of long needle-shaped particles and extrusion of the material contribute to the anisotropy of PGA graphite, a grade used in Mangox reactors in the United Kingdom.

2. Then the preferred coke is calcined at 1,300°C to remove a fraction of the volatiles contained in the material and to induce shrinkage.

3. Following the calcination process, the coke is milled and sized. These processes help maintain the uniformity of the coke particles.

4. The processed coke particles are then mixed with binder pitch, flour, or other carbon-rich materials.

5. Different forming processes can be chosen to shape the mixture of materials generated in the previous step. The formed material is known as *green article*. The forming process and raw filler materials influence the anisotropy of mechanical properties of the final product.

6. The green article is baked to further reduce the content of the volatile material.

7. Typically, coal-tar pitch is used to impregnate the baked article. The purpose of this step is to minimize the mixture's porosity content.

8. Finally, the baked green article is heated in a furnace that can reach graphitization temperatures (i.e., 2,500°C–3,300°C).

Additional details of graphite's manufacturing process can be found in the literature [3, 7].

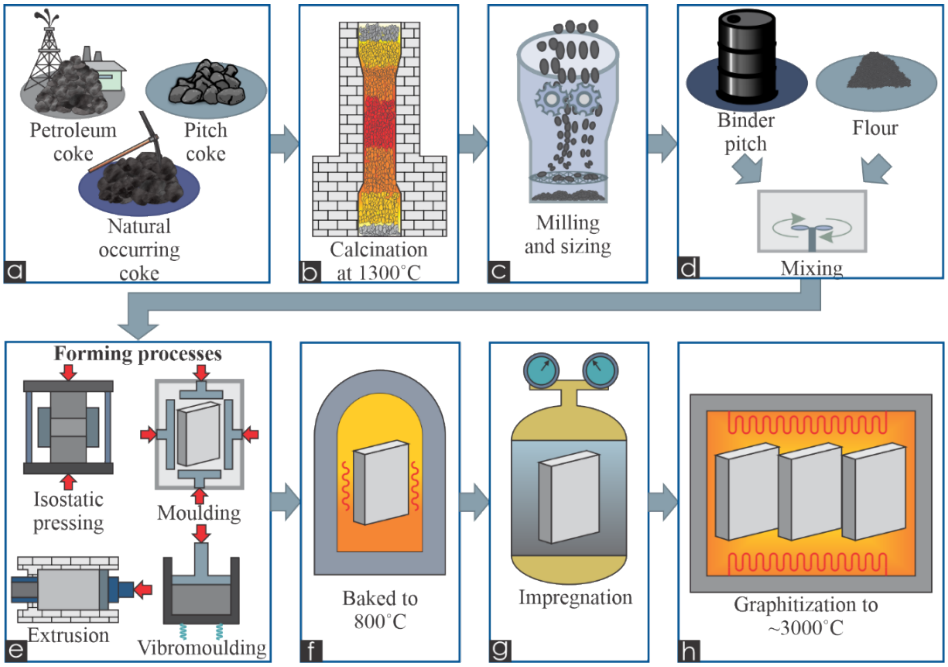

Figure 1. Raw materials and manufacturing processes of graphite.

2.2 MICROSTRUCTURE OF GRAPHITE

Graphite raw materials and conventional nuclear-grade manufacturing processes aim to produce porous polycrystalline materials composed of filler and binder phases (Figure 2). In addition to these two phases, graphite contains a large amount of porosity. Filler particles can be preferentially aligned. Alternatively, they can have a random orientation, producing a more isotropic material. The isotropy or anisotropy of graphite depends on the types of coke source raw materials and forming methods used to produce the graphite billets. By contrast, the crystallites for the binder phase are generally randomly orientated. Porosity in nuclear graphite strongly influences the bulk material properties, the irradiation-induced volumetric changes, and the potential failure of the graphite components. Porosity can constitute about 20% of the bulk volume. Pores can be as small as a few nanometers up to a few millimeters, depending on the grain size. Larger pores (>100 μm) dominate most of the mechanical properties in graphite, whereas smaller pores (<0.1 μm) are believed to control the irradiation-induced dimensional change, coefficient of thermal expansion (CTE), and thermal conductivity. In general, the porosity in graphite can be classified into three types: gas-entrapment pores (or gas-escape pores), shrinkage (thermal) cracks, and unfilled pores [8]. The gas-entrapment pores and shrinkage (thermal) cracks constitute most of the porosity structure in graphite. The influence of smaller pores on graphite's mechanical and physical properties remains to be fully understood. The off-gassing of the binder phase generates gas-entrapment pores during the baking stage [8]. The gas-entrapment pores are open (i.e., accessible to the atmosphere) and do not accommodate thermal expansion because they are relatively large; however, they do affect properties such as strength, thermal conductivity, and Young's modulus, particularly under radiolytic oxidation during reactor operation [9, 10]. Shrinkage (thermal) cracks are primarily formed because of the anisotropic CTE of the crystal structure and consequent internal stress relaxation when crystalline graphite is cooled from temperatures above 2,000°C. The CTE is higher in the crystallographic *c*-direction (20×10^{-6} to 40×10^{-6} K^{-1}) than in the *a*-direction (1.5×10^{-6}). The internal stresses act on carbon bonds between crystallites and the Van der Waals forces between basal planes [11]. This internal stress is usually relieved between the weakly bound basal planes. The shrinkage cracks usually have lenticular features that range widely in size from less than 5 nm to 200 nm in width and up to 10 μm in length and can be further classified into two categories: intragranular and intergranular. The intragranular

cracks are also referred to as *Mrozowski cracks*, and they are found within the filler crystallites and lie perpendicular to the crystallographic *c*-direction. The intergranular cracks lie between filler phase crystallites at grain boundaries. In principle, neighboring basal planes have no specific orientation. However, depending on the orientation of the sources of the filler materials (i.e., petroleum or pitch cokes) and forming process, the intergranular cracks usually either align perpendicular to the basal plane in the anisotropic filler phases or are randomly distributed without preferred orientations. Furthermore, within thermally anisotropic filler particles, closed calcination cracks (i.e., not accessible to the atmosphere) form because of volumetric shrinkage during the calcination stage in the manufacturing process [12].

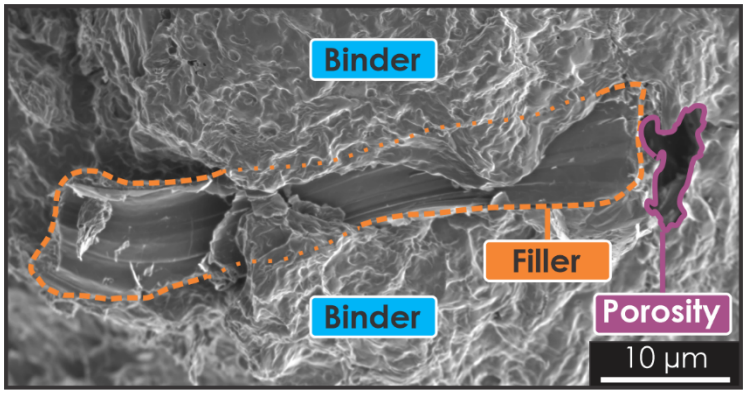

Figure 2. Scanning electron microscopy (SEM) micrograph of a fracture surface of graphite. This micrograph shows the three main phases of nuclear graphite: binder, filler and porosity.

The size of the filler phase defines the graphite grain size. Starting mix comprising grains substantially larger than 4 mm yields coarse-grained graphite. Starting mix comprising grains generally less than 4 mm yields medium-grained graphite. Starting mix comprising grains generally less than 100 µm yields fine-grained graphite [13]. Nuclear graphites generally have medium and fine grain sizes. The influence of smaller pores on graphite's mechanical and physical properties remains to be fully understood.

Graphite's complex microstructure cannot be fully characterized by a single microscopy technique and thus calls for a multiscale approach. The presence of different pore sizes and phases in graphite necessitates a wide range of microscopy techniques that enable the characterization of all the different aspects of nuclear graphite. Moreover, the complex microstructure also calls for a multidisciplinary approach, encompassing basic science on a structural scale (Figure 3). This project aims to combine the knowledge of all these scales and disciplines by providing data and guidelines and developing new techniques to understand graphite and the effect of the reactor environment on nuclear graphite.

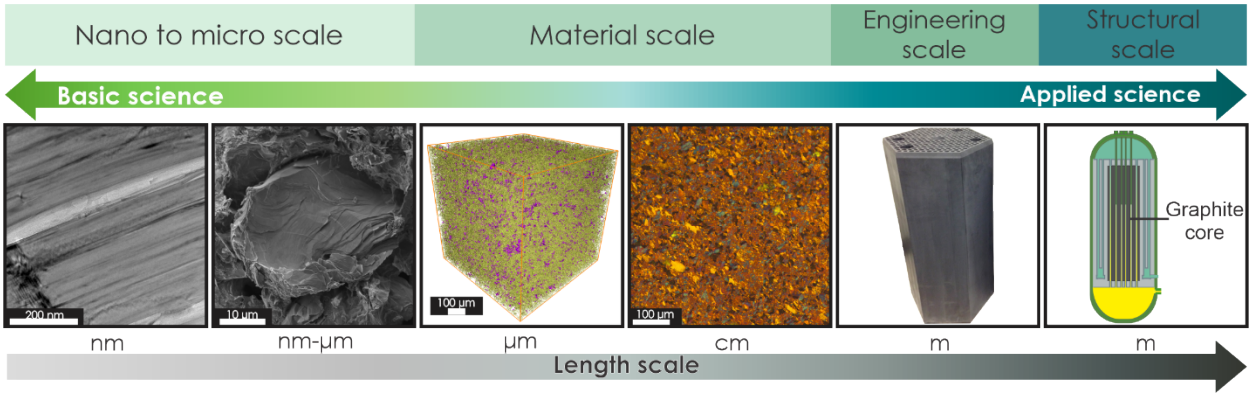

Figure 3. Multiscale nature of nuclear graphite. Challenges related to the understanding and characterization in nuclear graphite.

3. GUIDELINES FOR MICROSTRUCTURAL CHARACTERIZATION OF NUCLEAR GRAPHITE

Several ASTM International (ASTM, formerly American Society for Testing and Materials) guidelines exist to standardize the characterization of certain aspects of graphite such as density, mass, and overall qualification. However, these guidelines do not cover other essential characterization techniques commonly used to study nuclear graphite and the effects of the reactor environment on graphite components. A journal publication is being prepared to further explore the limitations and advantages of some standard techniques used to characterize graphite. Each technique has been used to study certain aspects of graphite, such as the pore size distribution, crystallinity, or 3D pore structure of the pores.

However, a technique/review paper has not thoroughly written to critic or comment on the characterization of graphite. The following subsection outlines some of the initial efforts to generate a guideline for some techniques. This initial effort will be further expanded to cover other analytical techniques and microscopy techniques shown in Figure 4.

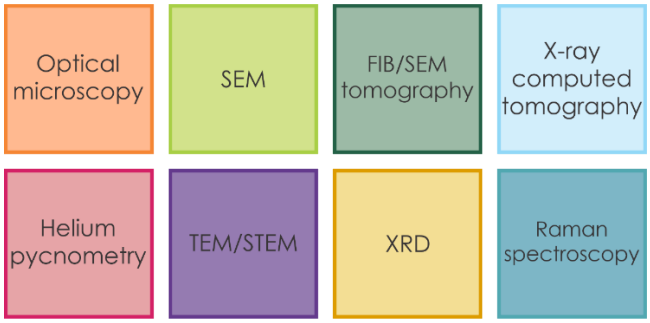

Figure 4. Examples of common characterization techniques used to characterize graphite.

3.1 ON THE USE OF MICROSCOPY TECHNIQUES AND ANALYTICAL TECHNIQUES FOR NUCLEAR GRAPHITE – A REVIEW

This outline surveys several techniques commonly used to characterize the microstructure, pore structure, and phases (binder and filler). Describing the advantages and limitations of some standard techniques allows for enhancing the characterization and understanding of irradiation effects on nuclear graphite. This initial guideline covers three techniques: optical microscopy, scanning electron microscopy (SEM),

and transmission electron microscopy (TEM). Each subsection summarizes a literature review of research that employed each technique.

3.1.1 Optical Microscopy

Several researchers have used optical microscopy to characterize graphite's porosity content and morphology. This technique can offer a first glimpse of the microstructure and provide essential metrics of the graphite's porosity content. Optical microscopy is often used to characterize the effects of oxidation on graphite because it can cover large areas by stitching multiple micrographs. Conventional mechanical polishing is the most common sample preparation technique for optical microscopy for nuclear graphite research.

Optical microscopy in nuclear graphite research is normally used for two purposes: to acquire grayscale images to analyze porosity and to produce micrographs in polarized mode for phase identification. Grayscale images can be segmented via thresholding techniques to quantify the porosity content in graphite and to study the morphology of the filler and binder. Conventional grayscale optical microscopy is often used to measure the porosity content of graphite before and after oxidation. In some graphite grades, such as fine-grade graphites, identifying filler and binder can be difficult under grayscale settings. Polarized optical microscopy enhances the contrast between domains that have different crystal orientations, facilitating the identification of the filler and binder regions. Polarized optical microscopy is perhaps the best technique for graphite phase identification for features larger than 10 μm. However, most of the analysis for phase identification with polarized light is limited to manual measurements of the filler particle size. Manual filler particle size measurements can be biased by user experience. The advent of artificial intelligence or heuristic methods may lead to more automatic and systematic identification of filler particles. Another issue with polarized optical microscopy is the colors in the micrographs can create difficulties during thresholding porosity analysis. This issue can be overcome by converting the color images to grayscale images. Figure5 shows examples of grayscale and polarized optical microscopy images.

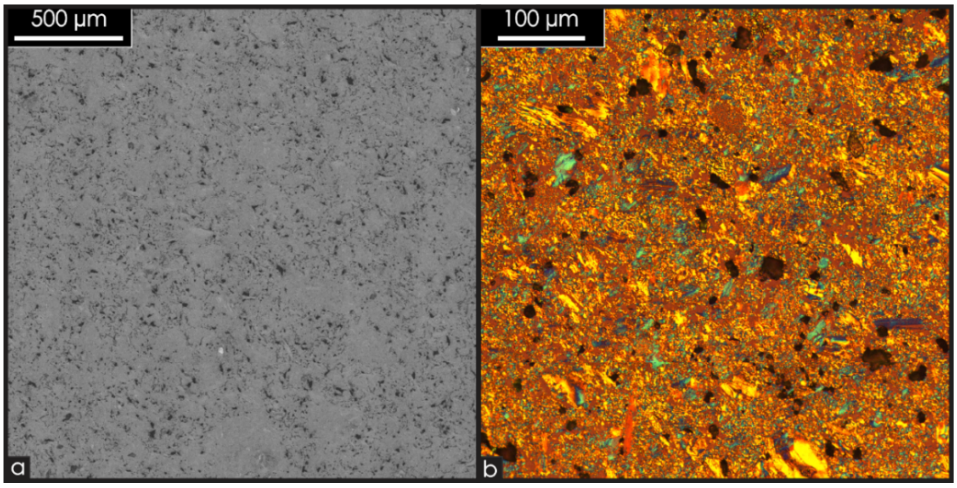

Figure 5. Optical micrographs of graphite. (a) Greyscale image of IG-110 and (b) Polarize micrograph of IG-110.

A general disadvantage of optical microscopy is the pixel size resolution. The wavelength spectrum of visible light limits this technique; therefore, some small cracks or features cannot be fully resolved. For example, the resolution of optical microscopy for an ultrafine POCO graphite grade such as ZXF-5Q may render these microfeatures difficult to distinguish. Therefore, some small pores may not be captured, so other techniques, such as SEM, may be required. Limited imaging resolution can also affect the pore

count at some magnifications; large data sets are required to mitigate this limitation. Table 1 summarizes relevant publications that discuss optical microscopy to characterize nuclear graphite.

Table 1. Summary of publications that discuss optical microscopy

Author(s)	Year	Ref.	Description
Burchell	1996	[14]	Optical micrographs and porosity analysis are used as inputs for a microstructural fracture model known as Burchell model.
Contescu and Burchell	2009	[15]	Optical micrographs and analysis of pore structure evolution of PCEA graphite, before and after oxidized in air to various levels of weight loss (5%–20%) and at three oxidation temperatures (600°C, 650°C, and 750°C).
Kane et al.	2011	[16]	This monograph details filler particle size measurements and an analysis of the porosity of four nuclear graphite grades.
Wang et al.	2012	[17]	Optical microscopy was used to analyze the evolution of porosity of IG-110 in a temperature range of 600°C–750°C.
Contescu et al.	2012	[18]	This research combines optical, x-ray diffraction, and Brunauer–Emett–Teller methods to analyze the oxidation resistance of three nuclear grades.
Manuwong et al.	2013	[19]	Calculations and pore size distribution of Gilsocarbon graphite grade are provided in this paper.
Takizawa et al.	2013	[20]	Measurement and comparisons of pore sizes and distribution, aspect ratios, ratio of total pore area to surface area, and ratio of total pore volume to sample volume using different techniques: optical imaging, mercury porosimetry, and Raman spectrometry, from two as-fabricated fine-grained nuclear graphites, G347S and G458S.
Metcalfe and Tzelepi	2015	[21]	This article provides a qualitative assessment of the microstructure of as-received Gilsocarbon samples as well as specimens exposed to neutron irradiation and oxidation.
Huang and Tang	2019	[22]	Measurement of gas-escape pore size and distribution of two fine- and ultrafine-grade graphites by optical microscopy and comparison of results with those from x-ray computed tomography and mercury porosimetry.

3.1.2 Scanning Electron Microscopy

SEM has been used extensively to analyze polished surfaces (Figure 6a), oxidized specimens, fracture surfaces (Figure 6b), crystallinity, and graphite microstructure. This versatile technique can capture large features such as large thermal cracks or gas-evolution porosity in coarse graphite grades (millimeters range) to small thermal cracks contained in the binder phase (micrometers range) (Figure 6b). High-resolution SEM micrographs can capture graphite's layered structure; some examples are provided in Figure 6c. Modern SEM instruments can operate at high (30 kV) and low (1–2 kV) acceleration voltages, allowing different levels of interaction between the electron beam and the graphitic structures (Figure 6c). Examples of the influence of acceleration voltage in SEM imaging for highly ordered pyrolytic graphite (HOPG) are provided in Figure 6c. High acceleration voltages can provide a better sense of depth and contrast than lower voltages. However, graphitic layers can appear transparent at high acceleration voltages.

In some cases, lower acceleration voltages in high-resolution SEM can enable studying the first graphitic layers of material. Sample preparation is another critical aspect of using SEM. The most common surface preparations are polished, fractured, and oxidized surfaces.

- Polished surfaces offer a clear view of the material's porosity content and can typically cover most of the length scales needed to characterize graphite. SEM images of polished samples can be used to study the porosity content in a sample. The main disadvantage of a polished graphite sample is the alteration or removal of certain features that complicate the identification of filler and binder phases.

- Fractured surfaces provide a clearer view of the filler and binder regions for SEM phase analysis. Fractured surfaces expose filler and binder regions, facilitating the identification of these phases. However, identifying pores in a fractured surface may be challenging because of the sample's complex topography. The fracture mechanisms used to obtain the surface can create a step surface. Another factor that influences the aspect of the fractured surface is the fracture mechanism and fracture mode implemented to obtain the fracture surface. Some fracture tests can privilege the fracture of the binder regions, leaving the filler particles intact. In some cases, round particles are not exposed, so only the outer face of the particle is exposed.

- Oxidized surfaces can remove some damage created by a sample's machining, polishing, or fracture. The oxidation process can create more pristine graphite surfaces. A drawback of this type of sample preparation is the preferential oxidation caused by certain metals that serve as catalysts during the oxidation process.

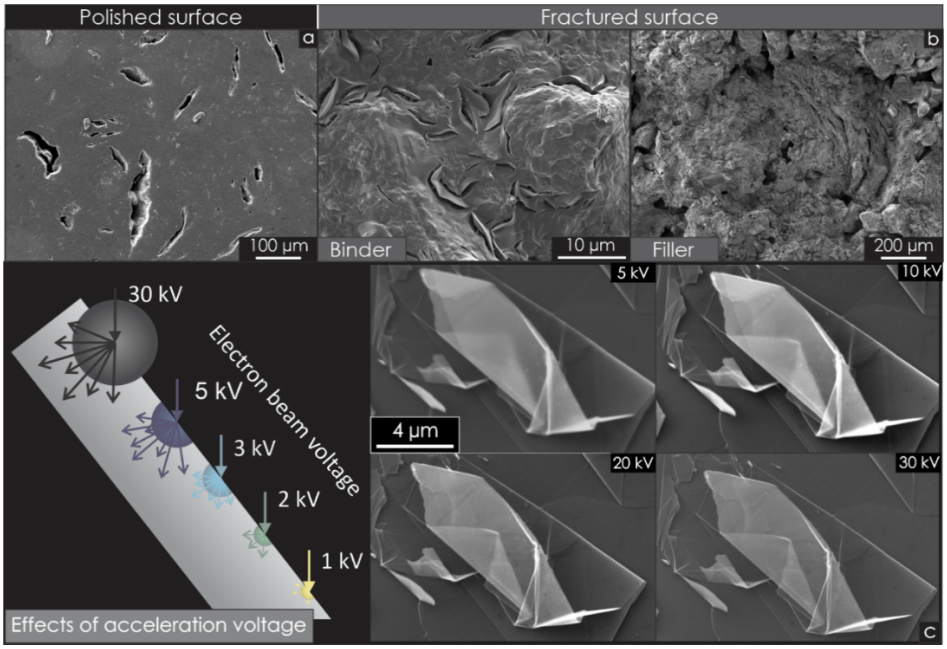

Figure 6. SEM micrographs of graphite. (a) SEM micrograph of a polished sample of NBG-17. (b) Fractured samples of NBG-17 filler and binder, and (c) penetration of electron beam in a sample and comparison of the effects of acceleration voltage in a HOPG specimen.

SEM is not used as extensively as other characterization techniques; however, this technique is commonly used to support other studies. Table 2 summarizes the most relevant publication on SEM for nuclear graphite characterization.

Table 2. Summary of manuscript covered in the SEM section

Author(s)	Year	Ref.	Description
Badenhorst	2017	[23]	This publication provides a comparison between SEM micrographs of oxidized surfaces of a natural graphite and NBG-18.

3.1.3 XCT and FIB-SEM Tomography

X-ray computed tomography (XCT) and focused ion beam (FIB)-SEM tomography are two 3D characterization techniques commonly implemented to characterize the porosity in graphite. Multiple researchers have adopted XCT to analyze the crack propagation in graphite [24, 25]. Segmented XCT data have been used to model graphite's properties or to analyze graphite's microstructure. In particular, XCT scans can be processed by imaging processing software to obtain graphite segmentations of the pore content. Figure 7 shows a slice of XCT data of IG-110 and a segmentation of these data. This type of analysis has been extensively used to characterize other nuclear materials, such as silicon carbide composites [26, 27] or pyrolytic carbon [28].

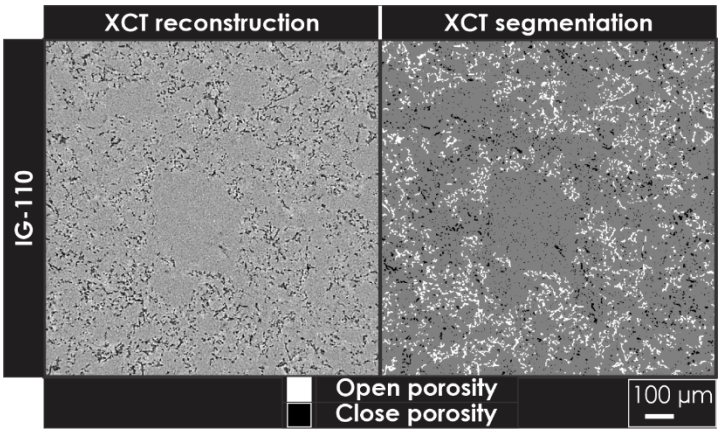

Figure 7. XCT slice of reconstructed data and respective segmentation. Data obtained from an IG-110 specimen.

FIB-SEM tomography is a technique that integrates the SEM and FIB to obtain high-resolution electron images of the surface of a region of interest. Figure 8 shows an example of a neutron-irradiated graphite sample (nominal irradiation temperature of 450°C, 29.8 dpa) of the superfine-grain graphite G347A (Tokai Carbon, Japan). Typically, an FIB is used to expose the desired region of interest, which is then imaged using the electron beam (Figure 8a). A sequential process produces serial images that can be processed (Figure 8b) and segmented to obtain detailed 3D models (Figure 8c). More information of the methodology to obtain this type of data can be found in the literature [29].

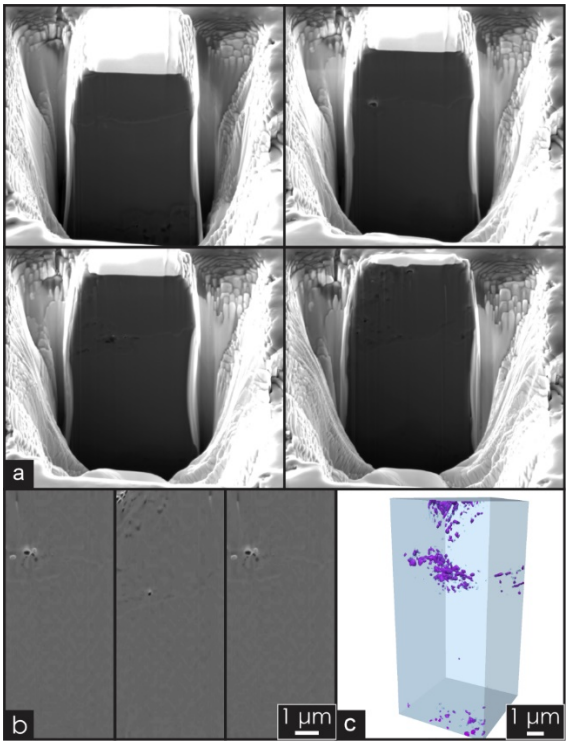

Figure 8. XCT slice of reconstructed data and respective segmentation. Data obtained from an IG-110 specimen. (a) SEM images, (b) cropped SEM images, and (c) segmentation of the porosity.

3.1.4 Transmission Electron Microscopy

TEM can analyze multiple aspects of graphite's morphology and directly analyze the irradiation effects in graphite. Compared with optical microscopy and SEM techniques, TEM resolution is high enough to present some fine structures within filler, binder phase, and a wide variety of pores, as well as crystallographic defects in graphite. Some specific features that can be better analyzed with TEM are Mrozoski nanocracks, crystal strain contrast, quinolone insoluble (QI) particles and chaotic structure in the binder phase, and turbostratic structures. Figure 9 shows bright-field (BF) TEM micrographs of NBG-17 grade graphite showing different microstructural features: interface region showing filler (marked F) and binder (marked B) (Figure 9a), filler particle containing Mrozoski cracks (Figure 9b), binder region containing rosette QI particle (Figure 9c) and a QI particle at high magnification (Figure 9d).

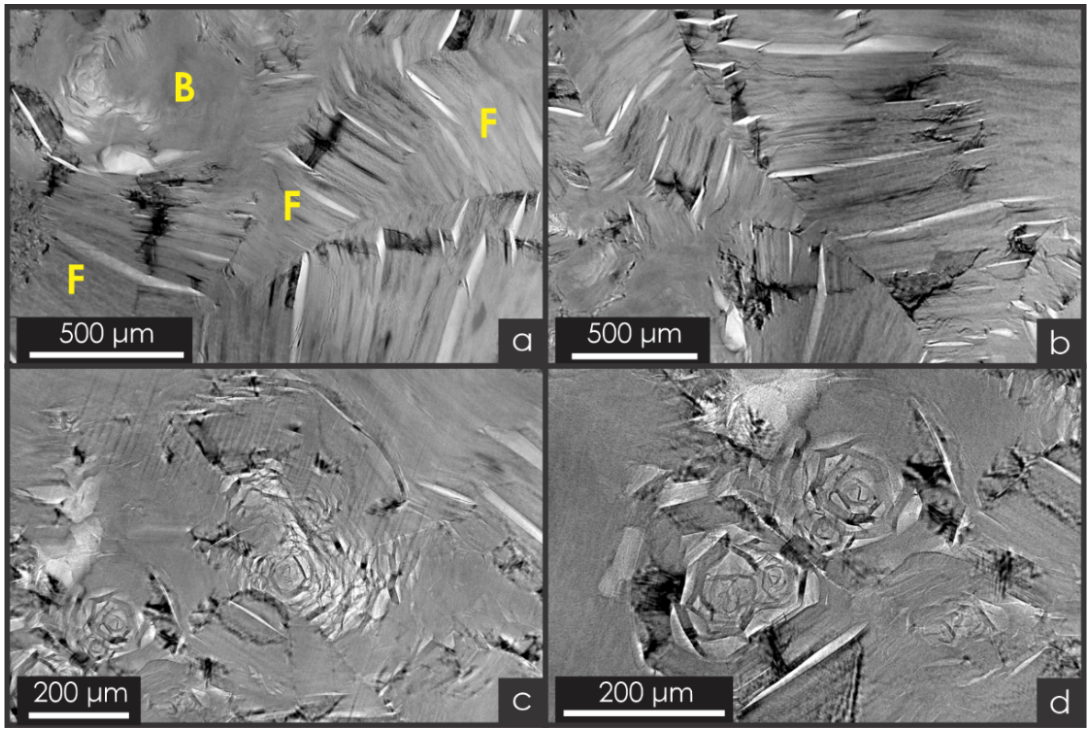

Figure 9. Bright-field TEM micrographs of NBG-18 grade graphite. (a) Interface region showing filler (marked F) and binder (marked B), (b) filler particle containing Mrozoski cracks, (c) binder region containing rosette QI particle, and (d) a QI particle at high magnification.

TEM is used extensively to characterize the phases and neutron-irradiation effects in nuclear graphite. The list of publications that cover this technique are given in Table 3 and Table 4.

Table 3. Summary of manuscripts covered in the TEM section (1990 to 2010)

Author(s)	Year	Ref.	Description
Koike and Pedraza	1994	[30]	This paper reports the microscopic dimensional changes and structural disordering observed in directions parallel and perpendicular to graphite basal plane of HOPG irradiated with 300 keV electrons at temperatures from 25°C to 657°C in TEM.
Shtrombakh et al.	1995	[31]	This paper presents the irradiation defects (dislocation loops and microcracks) in microstructures, linear and volume dimension changes, lattice parameters and Young's modulus changes under a wide ranges of irradiation temperature (500°C to 1,200°C) and neutron fluence (1×10^{28} to2×10^{26} n/m^2, E > 0.18 MeV) in pyrographites, nuclear graphite, and carbon graphite materials.
Burden and Hutchison	1998	[32]	This paper presents experimental evidence of single-shell fullerene formation on the surface of previously untreated KS10 graphite particles and Raven 430 carbon black particles, which were irradiated at 400 keV and temperatures of 500°C and 550°C in a controlled-environment high-resolution electron microscope (a gas-reaction cell with 5–25 mbar helium gas).
Wen et al.	2008	[33]	This article characterizes the aspect of cracks and their content as well as studies the closure of cracks owing to electron irradiation and thermal heating.
Karthik et al.	2011	[34]	This paper presents the vacancy and interstitial loop formation, swelling, and microcrack closing at the atomic level observed via in situ electron irradiation at room temperature in NBG-18 graphite.
Karthik et al.	2012	[35]	This article presents different features of the microstructure of three nuclear-grade graphites (IG-110, NBG-18, and PCEA) using the techniques of BF TEM imaging and selected area electron diffraction (SAED) pattern (i.e., the characteristics of filler and binder phases, microcracks, rosette-shaped QI particles, chaotic structure in binder phase, and turbostratic structure in filler phase).
Campbell et al.	2103	[36]	This paper presents a quantitative method to determine anisotropy from a pyrolytic carbon or ultrafine grain graphite using SAED patterns obtained by TEM. The analysis technique is integrated into a developed software program to quantify the anisotropy.
Mironov et al.	2015	[37]	This paper reports the atomic lattice structural and chemical bonding changes under electron irradiation at room temperature in PGA graphite. The irradiation damage is produced under 200 keV electrons up to a total dose of approximately 0.5 dpa.
Karthik et al.	2015	[38]	This paper reports the significant changes of microstructural features of NBG-18 and IG-110 after neutron irradiation to 6.78 dpa at 678°C, including the closure of microcracks in filler and binder phases and densified QI particles in the binder phase, as well as the formation of prismatic edge dislocations observed in HRTEM lattice images.
R. Krishna et al.	2015	[39]	This paper presents the microstructural changes of graphite samples irradiated at low temperatures of 20°C to 120°C, from samples removed from the British Experimental Pile Zero reactor at doses of 0.1, 1.3, and 1.45 dpa.

Table 4. Summary of manuscripts covered in the TEM section (2016 to 2021)

Author(s)	Year	Ref.	Description
Freeman et al.	2016	[11]	This article presents detailed characteristics within microcracks of filler particles from both unirradiated Pile Grade A and three irradiated British Experimental Pile Zero graphites using a combination of TEM, EELS, energy-dispersive x-ray spectroscopy and energy-filtered TEM techniques.
Freeman et al.	2017	[40]	In situ electron and temperature annealing experiments demonstrate the rate of generation of defects at different temperatures.
März et al.	2018	[41]	This article investigates the atomic arrangement and mesoscopic structure inside the filler and binder phases of Grade SNG623 graphite material.
Liu and Cherns	2018	[42]	This article investigates the nature of Mrozowski cracks and material inside these features by combining conventional BF TEM micrographs with scanning TEM (STEM) in medium angle annular dark field mode to examine Gilsocarbon grade graphite.
Johns et al.	2019	[43]	Specimens of IG-110 were exposed to a TEM electron beam to induce defects on a TEM lamella. The electron beam exposure caused so-called carbon onions or shelled fullerene phases to form.
Johns et al.	2020	[44]	This paper presents new fullerene-like microstructural defects observed in two high-temperature neutron-irradiated IG-110 samples, one irradiated to a dose of 1.73 dpa at 813°C and the other to a dose of 3.56 dpa at 817°C. Similar defects were observed in an unirradiated IG-110 under in situ electron irradiation.
Arregui-Mena et al.	2021	[45]	Electron tomography was adapted to characterize as-received and neutron-irradiated tips of nanocracks in IG-110. This article shows the 3D structure of the nanocracks found in graphite via 3D reconstructions obtained from different projections of images taken in STEM mode.
Liu et al.	2021	[46]	In this paper, ex and in situ ion irradiation using C^+ and Ar^+, respectively, are performed on HOPG at room temperature and 700°C. IG-110 underwent in situ electron irradiation at 300°C for dislocation characterization. The formation of surface vein structure and underneath triangular cracks were observed, and stress gradients were measured to be aligned with the vein structure. A macroscale ruck-and-tuck model is proposed as a feasible mechanism to explain dimensional and property changes in polycrystalline nuclear graphite.

3.1.5 Helium Pycnometry and Mercury Porosimetry

Determining graphite's mass is a simple procedure; however, the volume of graphite or solid content can be challenging to obtain because of its porous nature. In general, the porosity of graphite is classified as open and closed. Figure 10 shows the two types of graphite porosity and bulk volume.

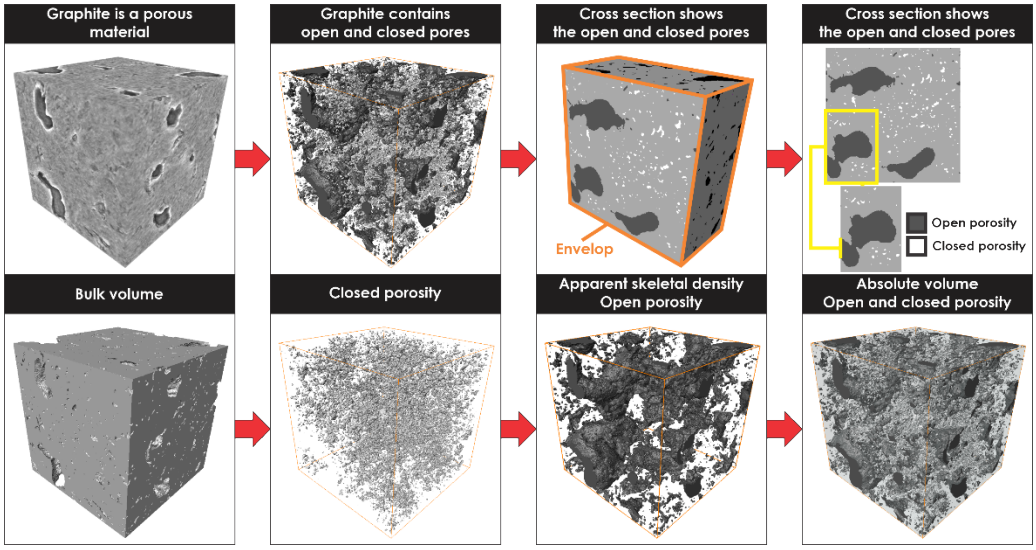

Figure 10. Porosity aspects of nuclear graphite.

Measuring the open porosity of graphite can be a simple task because the pores connect to the sample's surface, allowing for the use of gas or other medium to estimate the content of open porosity. Helium pycnometry and mercury porosimetry are normally used to estimate the skeletal density of a graphite sample. By contrast, mercury porosimetry is used to measure the pore size distribution. These measurements are normally complemented by dimensional inspections and mass measurements. Some of these techniques will be further explored to complement the 3D characterization techniques used in this research, such as XCT or FIB-SEM tomography.

4. LIBRARY OF MICROSTRUCTURES OF NUCLEAR GRAPHITE - STRUCTURE OF THE DATABASE AND DATA ACCESABILITY

Figure 11 summarizes the general outline of the library of microstructures. This database will comprise three main subsets: a baseline characterization of modern and historical grades; microstructural data of specimens exposed to neutron irradiation, oxidation, or both; and carbon-based materials used in the nuclear industry. The library would be supported by journal publications and reports that will explain the data and support the database. The following subsections provide an in-depth description and preliminary results of the publications and objectives of each library subset.

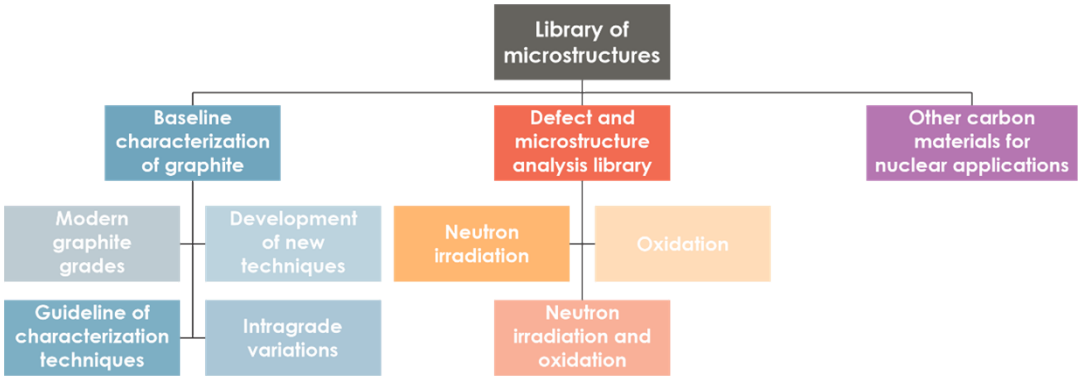

Figure 11. General structure of the library of microstructures.

4.1 ONLINE REPOSITORY

The following three strategies are being explored to store and document the data of the library of microstructures:

a) *Mendeley scientific database and Data-in-Brief publications*—The data of some of the publications that document and encompass these efforts are being stored in the Mendeley Data website and in conjunction with journal articles published as Data-in-Brief publications.

b) *Online website*—A website might be created to store and control access to the data and related information.

c) *Gen IV Materials Handbook for Very High Temperature Reactor (VHTR)*—The data and related publications might be incorporated into the Gen IV Materials Handbook Project.

5. BASELINE CHARACTERIZATION ON NUCLEAR GRAPHITE

This library portion focuses on the microstructural characterization of historical and candidate graphite grades of US nuclear graphite-moderated reactor designs. More in-depth characterization focused on the heterogeneity of graphite that arises from batch-to-batch productions of the same graphite grade. For this part of the research, PCEA graphite grade is characterized. This research's final element is a guideline describing the advantages and limitations of some of the most popular techniques used to characterize graphite. This guideline will support the qualification of graphite materials, helping regulators and the graphite community to understand the state of the art of different microstructural techniques.

5.1 LIBRARY OF MICROSTRUCTURES

The initial characterization of some of the historical and modern graphite grades have been covered in the following publications: "Multiscale characterization and comparison of historical and modern nuclear graphite grades" [47] and "SEM and TEM data of nuclear graphite and glassy carbon microstructures" [48]. In addition, CGB graphite, a nuclear grade designed for the Molten Salt Reactor Experiment, was extensively studied. This study elucidated the microstructure of this material and the sealant material used in CGB graphite [49].

The first two publications initiated the efforts to consolidate the first part of the library and are free to access online. The online repository of these publications is available at https://data.mendeley.com/datasets/z7gkhwg243/1.

This part of the project will be further expanded to characterize certain grades of interest for US reactor designs. The potential list of grades that will be further explored is listed in Table 5.

Table 5. Candidate grades selected for future characterization

Graphite grade	Coke source	Forming process	Type	Grain size (μm)	Manufacturer
2114	Nonpetroleum coke	Isostatically molded	Super-fine	13	Mersen
ETU-10	Coal-tar pitch	Isostatically pressed	Super-fine	15	Ibiden
IG-110	Petroleum coke	Isostatically pressed	Superfine	20	Toyo Tanso
PCEA	Petroleum	Extruded	Medium-fine	800	Graftech
NBG-18	Pitch	Vibromolded	Medium-coarse	1,600	SGL, carbon

5.1.1 Intragrade Variations of Microstructural Characteristics and Distribution of Properties for PCEA Nuclear Graphite

Manufacturing methods and raw materials can affect graphite's heterogeneity and microstructural characteristics. Even with similar production conditions and raw materials, material variability can be present within a billet, between billets, and between different batches of graphite [50, 51]. This part of the project will assess batch-to-batch intervariability using PCEA graphite. Moreover, this research will establish protocols to identify critical differences and determine whether these variations are significant. Significant batch-to-batch intervariability increases the uncertainty of irradiation behavior predictions between past and modern versions of the material.

Evaluations and characterization of PCEA graphite were performed on three batches produced at various times to examine the variations among these materials. ORNL and Idaho National Laboratory collaborated on these efforts to establish criteria, analysis frameworks, and tools for manufacturers and reactor designers to identify and quantify variations between graphite batches. Additionally, the characterization conducted in this research is being incorporated to expand the library of microstructures for US graphite programs. Several techniques were employed in this study, including SEM, helium pycnometry, x-ray diffraction, XCT, and ultrasonic measurements for elastic modulus data.

Previous measurements performed at Idaho National Laboratory covered the physical and mechanical properties. These results indicated some degree of mechanical property variations among the three PCEA graphite batches. To gain a better understanding of these material variations, the surfaces of fractured samples are being examined using SEM. Figure 12 shows the three phases of graphite: the binder, filler particles, and a QI particle. In Figure 12, the binder phase of PCEA's surface resembles a molten substance, partially covering a section of the filler particle. Other sections of the binder material in PCEA show significant cracks and pores resulting from the various heating manufacturing processes. The PCEA filler particles possess needle-like shapes with multiple corrugations along their length and sides. Stacked layers of graphite sheets are randomly intertwined and combined, defining the specific grade. The final phase, QI particles, consists of an outer shell composed of graphitic structures with internal cracks resembling a rosette shape (Figure 12).

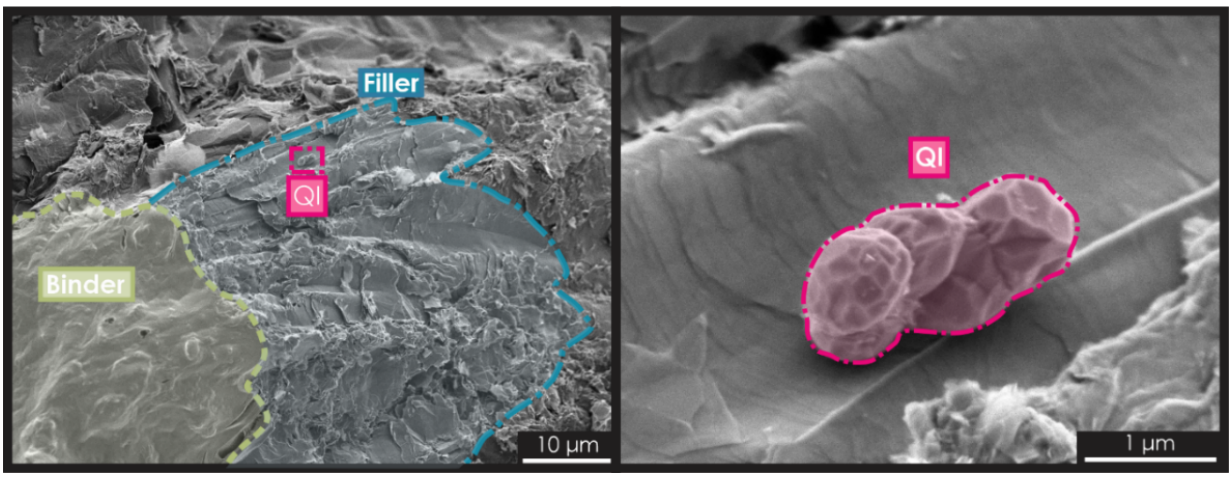

Figure 12. SEM micrographs of the phases of PCEA graphite. Binder, filler particles, and a quinoline insoluble (QI) particle.

Fracture surfaces of the three PCEA batches were systematically imaged to identify the phases illustrated in Figure 13. These observations aimed to identify any significant morphological changes in the phases of PCEA graphite. Figure 13 shows the filler particles of the three PCEA batches. The left column of Figure

13 shows low-magnification micrographs of the filler particles, and the right column shows corresponding high-magnification views. In general, the surfaces and texture of the filler particles exhibit nearly identical morphologies.

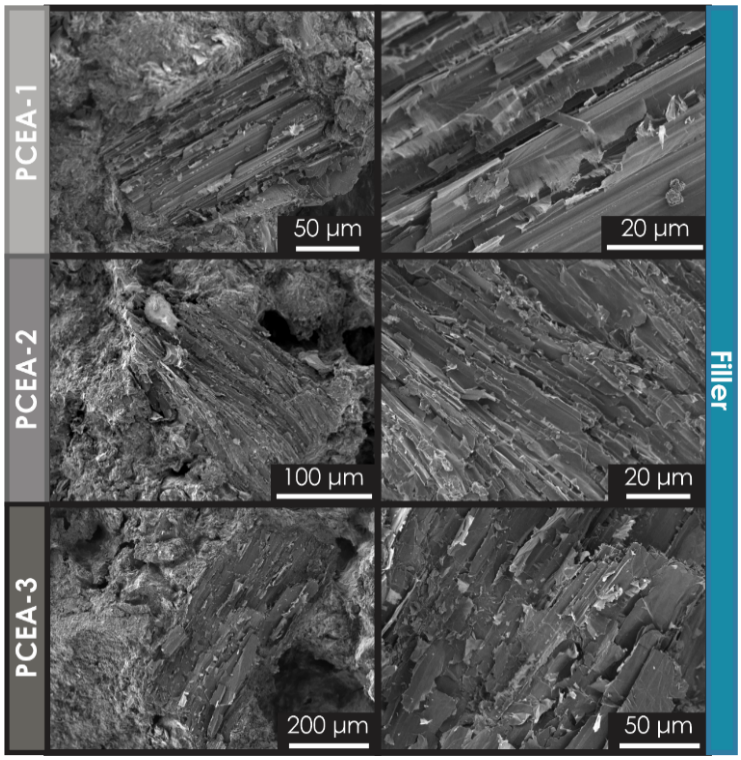

Figure 13. SEM micrographs of the three PCEA graphite batches. These images illustrate the surface and morphology of filler particles in PCEA graphite.

Similarly, the binder surfaces of the three PCEA samples were characterized. Like the filler particles, the binder materials for the three PCEA types appear highly similar, as shown in Figure 14. The three graphite batches contained large portions of binder material with thermal cracks of various sizes.

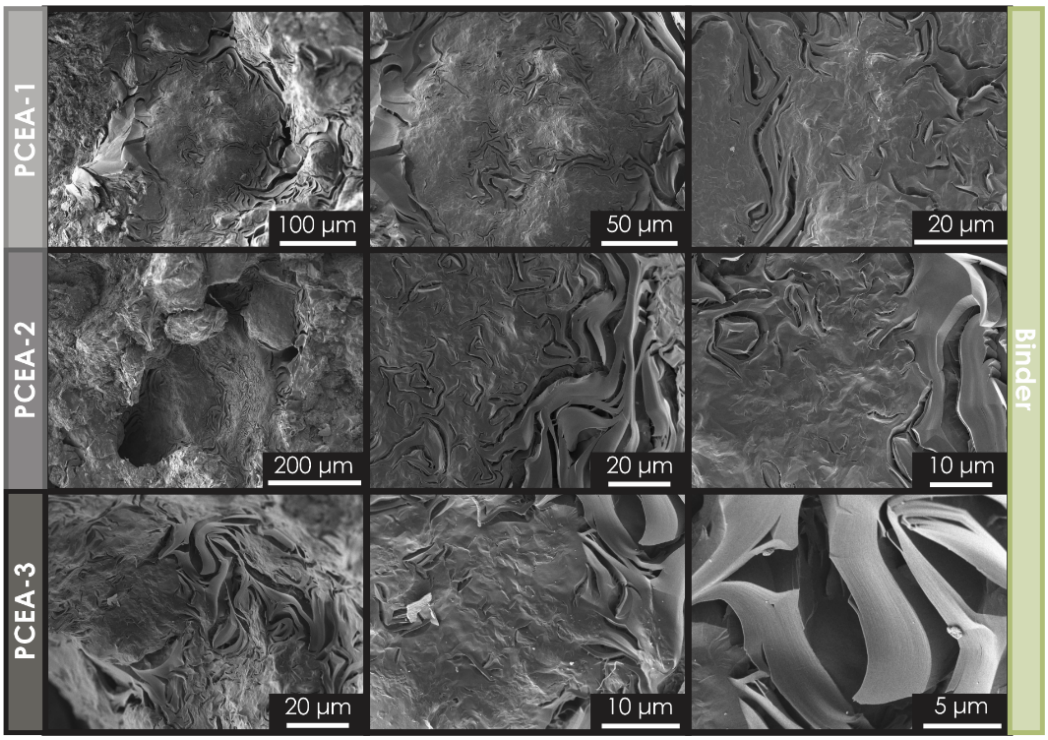

Figure 14. Micrographs of the binder phase of the three PCEA graphite batches. The SEM micrographs reveal that the binder phases are similar and contain similar range of crack sizes.

Figure 15 shows that the three PCEA types had similar quantities and distributions of QI particles. QI particles were classified based on their location, size, and quantity. This classification included QI particles embedded in the binder, large QI particles randomly scattered in the material, and large pockets of QI particles. QI particles embedded in the binder were relatively small, ranging from 200 nm to a few micrometers. These types of QI particles are typically present in crack-free regions of the binder. Larger QI particles (10 µm) appeared to be randomly scattered on the surface of PCEA and were usually isolated. Pockets of QI particles were found near the binder phase and exhibited a wide range of particle sizes. Figures 13 and 14 support the notion that the overall composition of raw materials was similar among the three PCEA batches. However, further microstructural characterization will be conducted to elucidate the variations contributing to differences in the mechanical properties of PCEA.

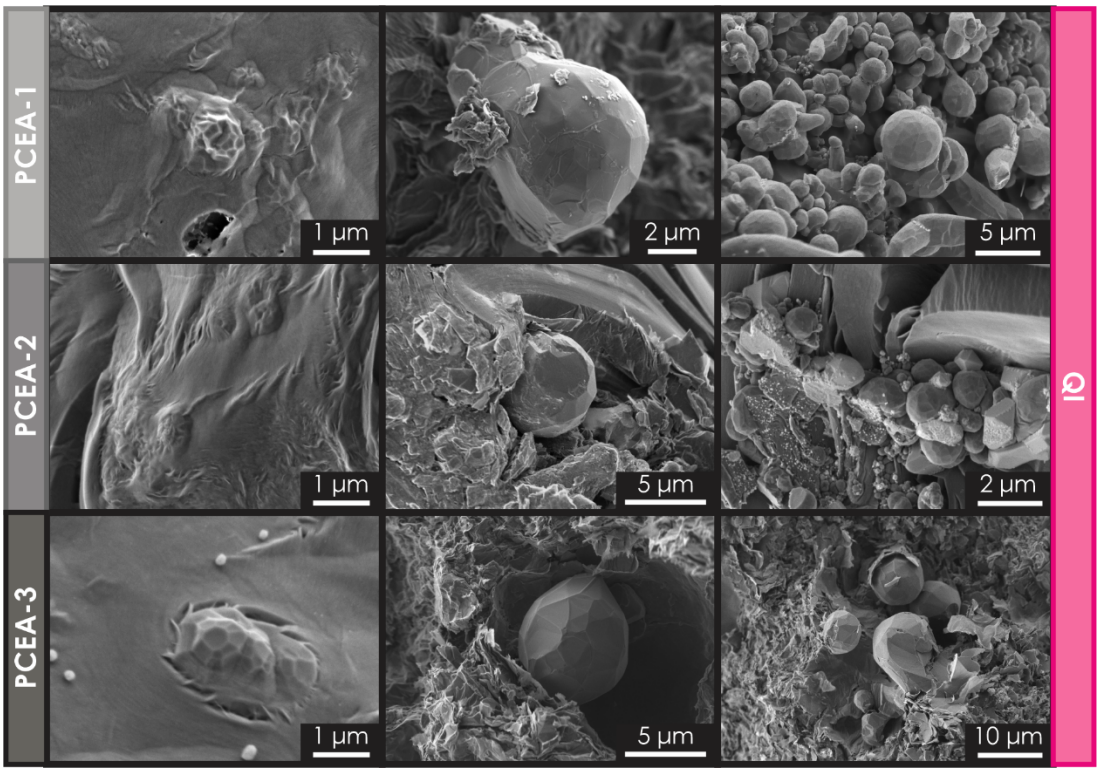

Figure 15. Micrographs of the quinoline insoluble phase of the three PCEA graphite batches. The overall distribution and texture of the quinoline insoluble appear to be the same between the batches.

Helium pycnometry measurements were conducted on samples of PCEA to assess the differences between open porosity and skeletal density. The helium pycnometry results are listed in Table 6. The highlighted specimens represent the samples with the lowest density (blue), the specimen with values close to the average density (green), and the densest specimen (orange). These samples were selected for XCT analysis to evaluate the differences in the pore structure.

Table 6. Helium pycnometry results for the three productions of PCEA

PCEA-1			PCEA-2			PCEA-3		
Sample ID	**Weight (g)**	**Density (g/cm³)**	**Sample ID**	**Weight (g)**	**Density (g/cm³)**	**Sample ID**	**Weight (g)**	**Density (g/cm³)**
PCEA-1-1	1.3558	2.0689	PCEA-2-1	1.2853	2.1665	PCEA-3-1	2.2452	2.0944
PCEA-1-2	1.2876	2.0602	PCEA-2-2	1.2895	2.1900	PCEA-3-2	2.0436	1.9890
PCEA-1-3	1.3186	2.0539	PCEA-2-3	1.2994	2.0722	PCEA-3-3	2.2006	2.0830
PCEA-1-4	1.3423	2.1878	PCEA-2-4	1.3176	2.1221	PCEA-3-4	1.8388	2.1367
PCEA-1-5	1.2978	2.2686	PCEA-2-5	1.3445	2.1902	PCEA-3-5	1.9409	2.0811
PCEA-1-6	1.2983	2.0784	PCEA-2-6	1.3279	2.2673	PCEA-3-6	1.9712	2.1607
PCEA-1-7	1.3159	2.0121	PCEA-2-7	1.3709	2.0379			
PCEA-1-8	1.2723	2.2640	PCEA-2-8	1.3443	2.2879			
			PCEA-2-9	1.3231	2.2674			

Figure 16 shows the preliminary XCT results of the selected samples from Table 6. The scan views included in Figure 16 and other low-magnification scans are being examined to understand the pore

morphology in PCEA graphite. Microstructural variations in nuclear graphite might also affect the stress distribution of a graphite component under neutron irradiation.

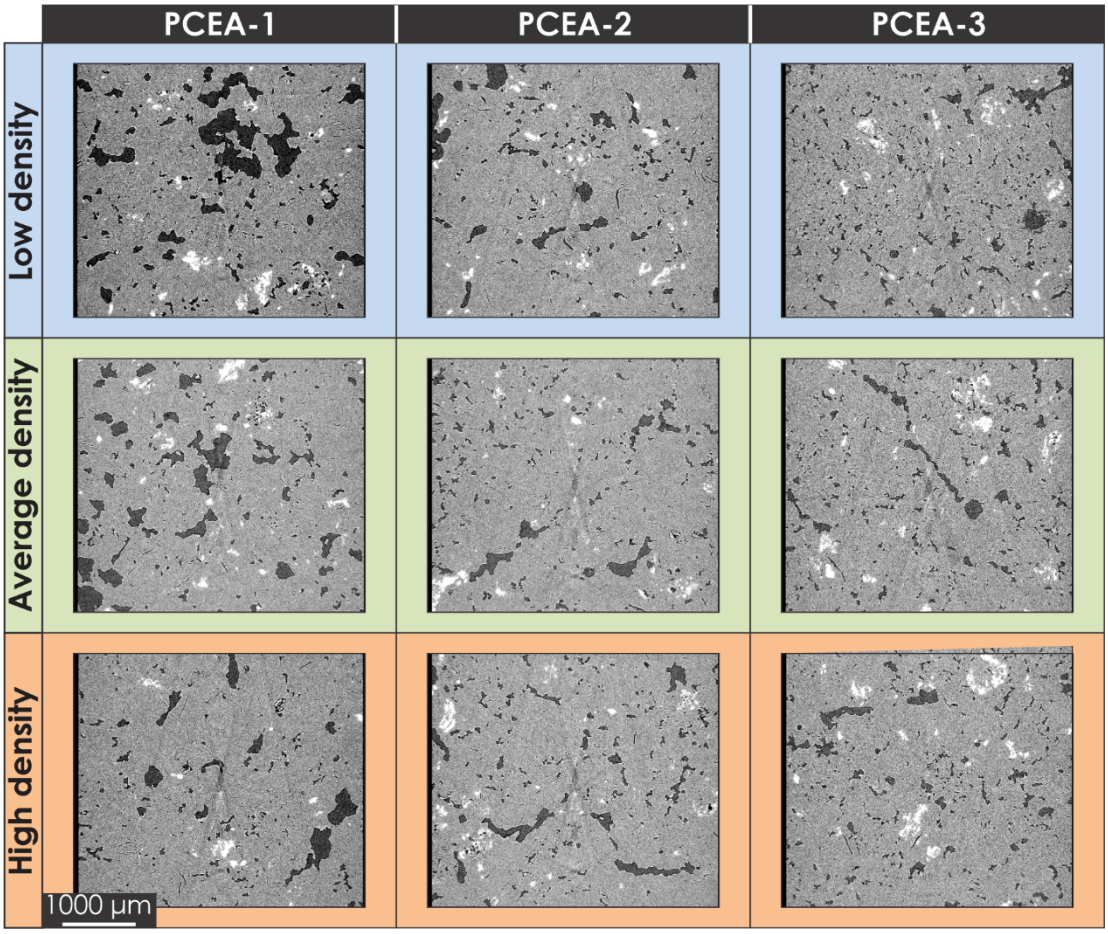

Figure 16. XCT reconstruction slices of three batches of PCEA. (top) Low-density samples, (middle) specimens close to the average density, and (bottom) high-density samples.

This research will be expanded to investigate how nuclear-grade graphite samples can differ across batches and will outline protocols to determine whether their differences are significant. For this purpose, the stochastic finite element method (SFEM) [52] will be adopted to compare how the variations of mechanical properties might affect the performance of the three grades. In the past, the SFEM framework has been adapted to characterize and capture the spatial material variability in graphite [5, 53].

So far, the collected data show that the batches shared similar microstructural characteristics. However, significant mechanical property variations must be investigated. These research data will be incorporated into the main library of microstructures of as-received material.

5.1.2 Characterization of Neutron Irradiation Effects, Machining, Polishing and Oxidation in AXF-5Q Graphite via Raman Spectroscopy

Raman spectroscopy is a common technique used to characterize the surface of nuclear graphite. In general, Raman spectroscopy can provide valuable insight into the damage caused by neutron or ion implantation. However, the technique is limited by the penetration depth into the material (estimated to be around 50 nm). This limitation might skew some of the results available in the literature. To show the

influence of the sample surface on the measurements, several surface and neutron-irradiation conditions were selected. Samples of AFX-5Q graphite, a binderless grade, were selected to reduce the uncertainty that arises from graphite material formed by filler and binder. Table 7 lists the probed surfaces.

Table 7. Types of surfaces probed for Raman spectroscopy

Surface type	Nonirradiated	Neutron irradiated	Oxidized
Fractured	Yes	Yes	Yes
Machined	Yes	Yes	Yes
Mechanically polished	Yes	Yes	Yes

The spectra included in Figure 17 demonstrate that neutron irradiation decreases the intensity of the G peak and increases in the signal of the D peak. Typically, an elevated D peak indicates enhanced disorder or damage to the graphite's crystal structure. By contrast, the G peak reflects the level of crystallite order. As shown in Figure 17a, the machined surface exhibits more damage than the fracture surface of the as-received sample. Figure 17b compares the damage incurred from the combined effects of neutron irradiation and machining with the damage caused by neutron irradiation. Machining introduces additional damage that affects the overall reduction in the signal of the G peak.

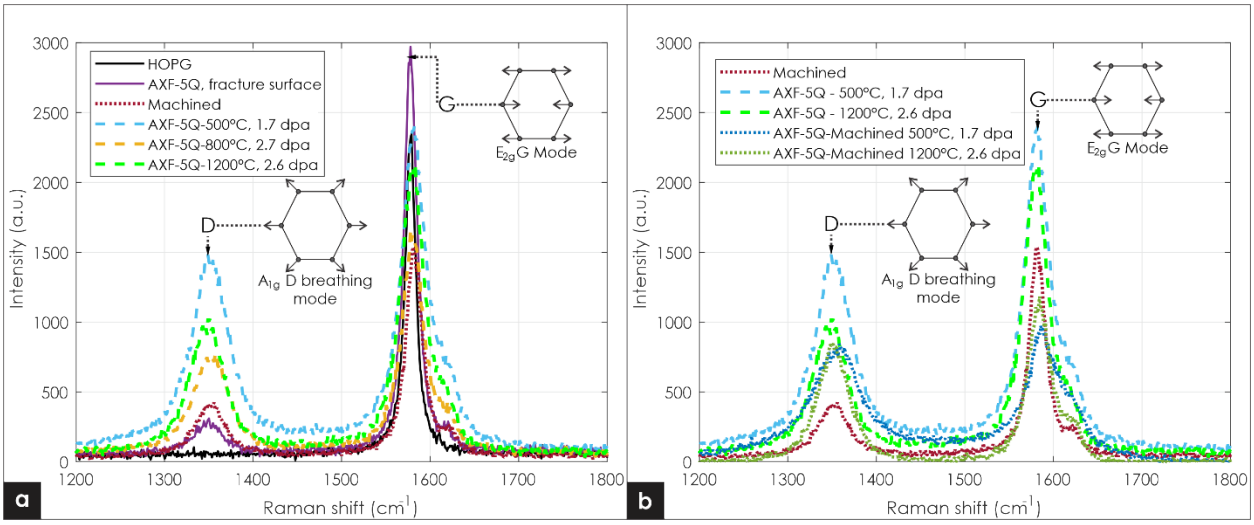

Figure 17. Raman spectroscopy results of neutron-irradiated materials. (a) Effects of neutron-irradiated materials in fractured surfaces and machined surfaces, (b) Combined effects of machining and neutron irradiation

These findings illustrate the potential of Raman spectroscopy to differentiate between regions of machined surfaces and areas unaffected by machining. However, these results illustrate the difficulty of distinguishing between damage resulting from neutron irradiation and that from machining. Additional surface types (oxidized and mechanically polished) are being probed to elucidate the role of the sample surface on Raman spectroscopy measurements.

5.1.3 Implementation and Development of New Techniques

Even with new techniques, several aspects of nuclear graphite remain to be discovered. Some irradiation effects, such as point defects or irradiation creep are not fully understood or characterized. Closing these knowledge gaps requires advancing the sample preparation and characterization techniques used to study the evolution of damage induced by the reactor environment.

Current efforts at ORNL will develop the techniques and analysis framework required to characterize and understand graphite microstructure in 3D. Various techniques are shown in Figure 18. Covering all of the features of nuclear graphite and the irradiation effects requires a multiscale approach. The techniques shown in Figure 18 can capture the pore size distribution of gas-evolution porosity (XCT, optical microscopy with mechanical serial sectioning, plasma FIB-SEM tomography), micropores and thermal cracks (FIB-SEM tomography and Nano-XCT), or irradiation effects and nanocracks (electron tomography).

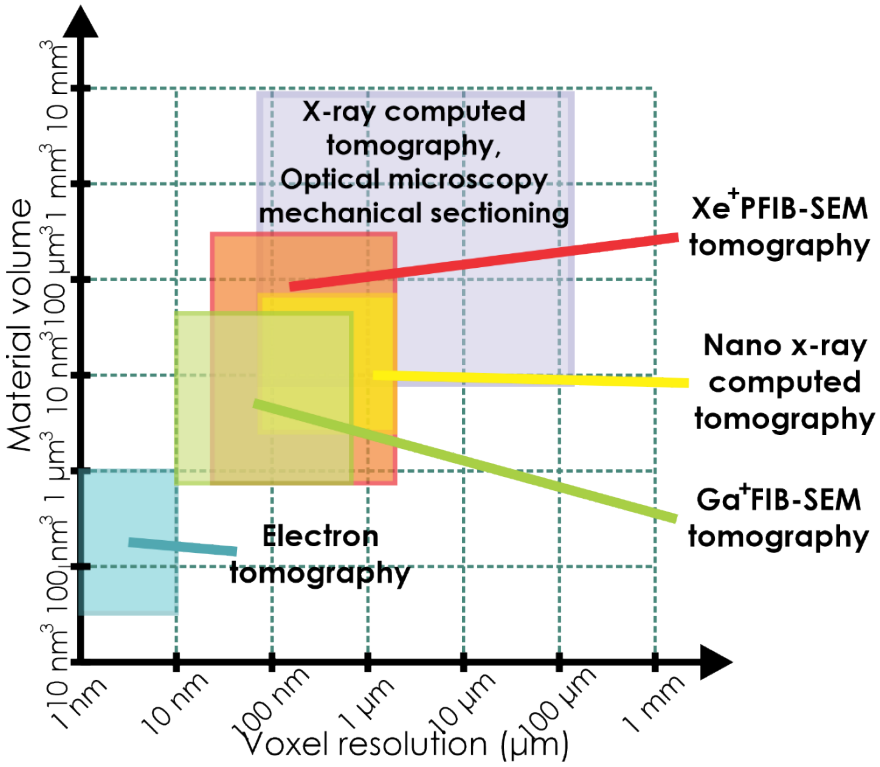

Figure 18. 3D Characterization techniques commonly used to characterize materials. These characterization techniques are being adapted to study nuclear graphite

The graphite grades included in Table 8 will be further characterized using some of the techniques shown in Figure 18. Plasma FIB (PFIB)-SEM tomography will be used to investigate graphite nanocracks and smaller void content in graphite. Optical microscopy/mechanical sectioning will be adapted to study the texture of filler particles of the selected grades. In addition to the 3D characterization techniques, ellipsometry [54] will be used to study the texture and anisotropy of these grades. These techniques are summarized in Table 8. The following subsections provide further details.

Table 8. Summary of future characterization techniques for selected graphite grades

Graphite grade	Coke source	Forming process	Type of characterization
2114	Nonpetroleum coke	Isostatic molding	PFIB, serial sectioning/optical microscopy, ellipsometry
ETU-10	Coal-tar pitch	Isostatic pressing	
IG-110	Petroleum coke	Isostatic pressing	
PCEA	Petroleum	Extrusion	
NBG-18	Pitch	Vibromolding	

5.1.3.1 Mechanical Serial Sectioning for 3D Graphite Microstructural Characterization

Serial sectioning is a promising technique to capture the 3D structure of nuclear graphite. This characterization method involves two simple iterative steps: mechanical polishing and optical imaging. The first step entails removing a specific amount of abrasive material to create a flat polished surface, and the second step involves capturing 2D characterization optical images after each section has been prepared. In this case, the material removal is achieved by polishing graphite using abrasive silicon carbide paper and diamond paste, and the imaging is done using optical microscopy. The automatic characterization by serial sectioning is made possible by a RoboMet3D system located at ORNL (Figure 19). The RoboMet3D is equipped with a polishing station, a robotic arm for sample handling, and an optical microscope.

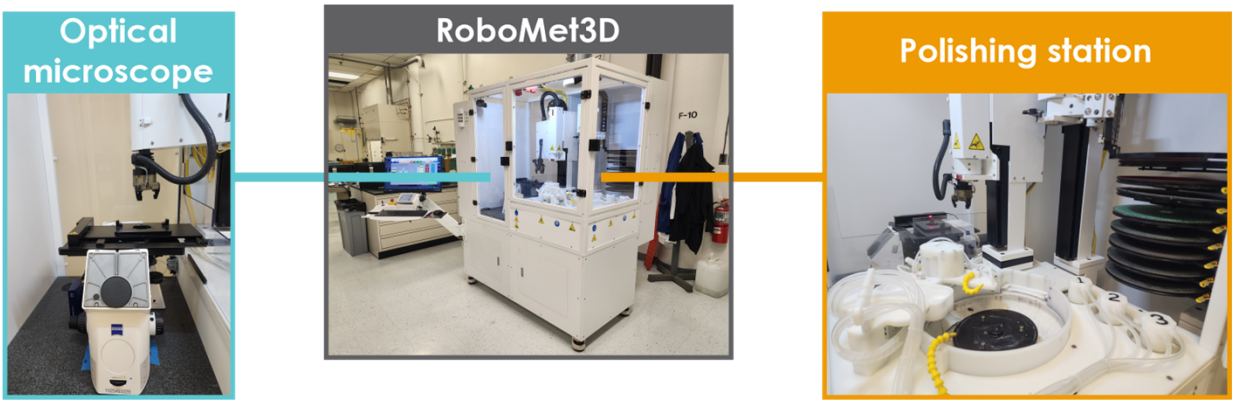

Figure 19. RoboMet3D serial sectioning machine and its components.

The ORNL team has conducted initial tests to establish parameters for removing approximately 2–5 µm of material per removal step for fine-grain graphites and around 10–20 µm for coarser grades. This characterization will facilitate the analysis of nuclear graphite filler, binder, and oxidation effects. Preliminary results from IG-11 are included in Figure 20.

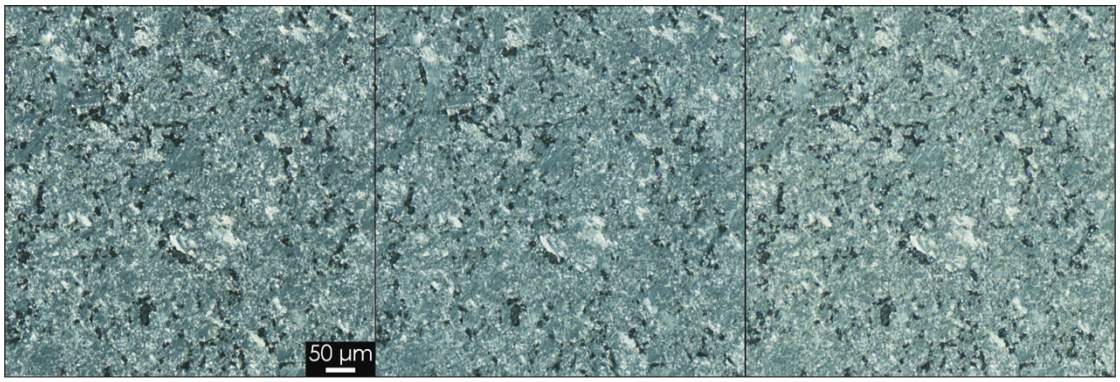

Figure 20. Optical micrographs of IG-11 obtained via serial sectioning.

5.1.3.2 Plasma Focused Ion Beam Scanning Electron Microscopy Tomography

In the past, FIB-SEM tomography was used to characterize the microstructure of unirradiated graphite and pyrolytic carbon [8, 28, 49, 55]. However, the volume that can be probed at a given time is limited by the milling rate of a traditional FIB. To improve the probed volume of interest, a PFIB will be used to examine the unirradiated microstructure of the selected grades. An example of the initial development of PFIB tomography developed at ORNL for a porous transport layer is given in Figure 21. These images

show the high-resolution images achieved by this technique and the large volume that can be characterized at a given time.

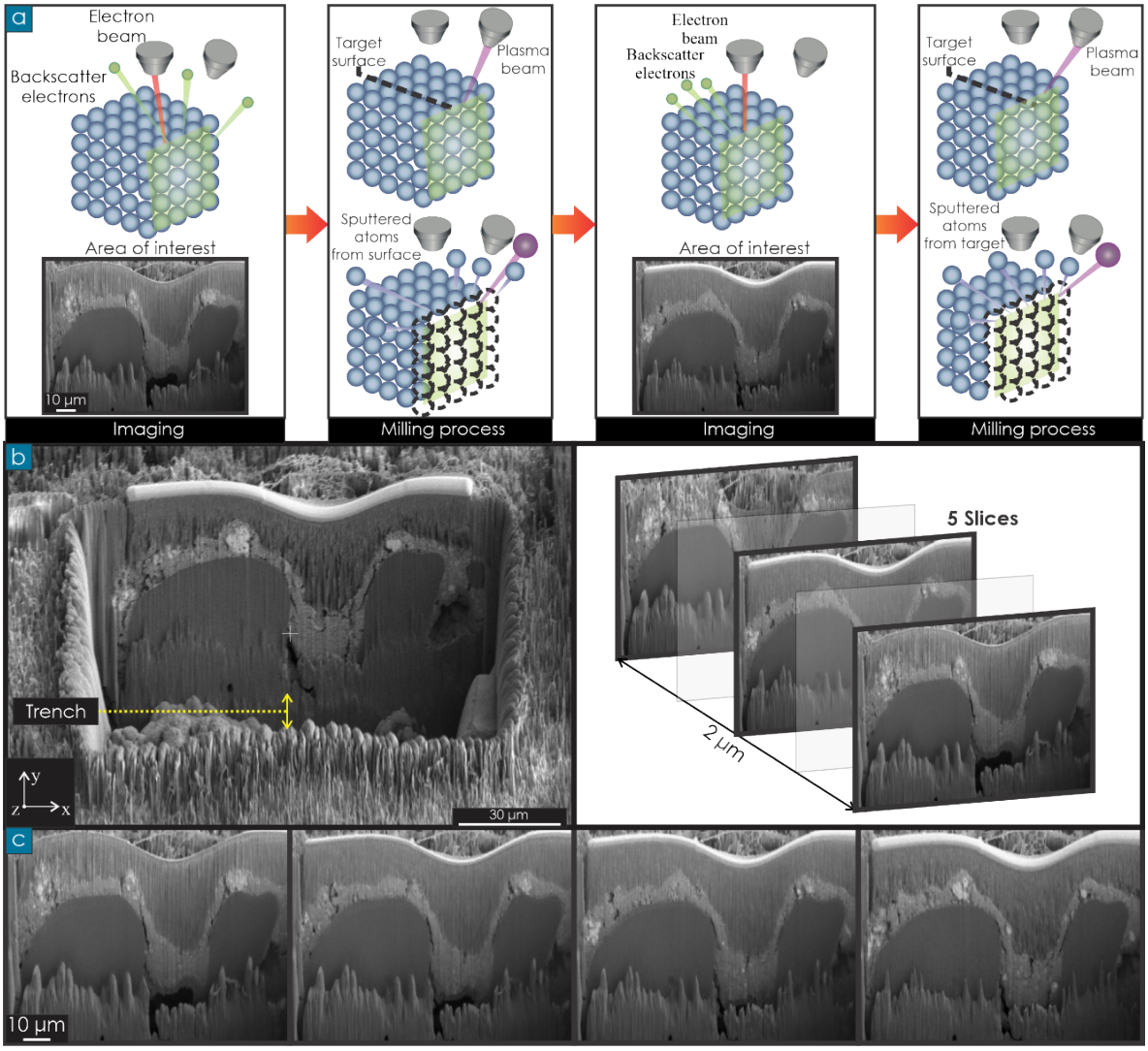

Figure 21. PFIB-SEM tomography methodology and result of the characterization of a porous transport layer. This technique is being developed as a collaboration between ORNL and the University of Tennessee. (a) Milling and imaging serial procedures to produce the SEM micrographs, (b) prepared surface and example images of PFIB-SEM tomography, and (c) Representative image results of PFIB-SEM tomography

Moreover, PFIB-SEM tomography will be adapted to study the penetration depth of molten salts into graphite. SEM imaging and energy-dispersive x-ray spectroscopy will also be used to measure the penetration depth of molten salt into different grades of nuclear graphite.

5.1.3.3 Ellipsometry

Ellipsometry can be used to analyze the local orientation of graphite phases by measuring the optical diattenuation of the selected graphite grades. *Diattenuation* is a metric related to the average orientation of the graphitic planes. A more detailed description of this technique is available elsewhere [54]. In this research, the grades listed in Table 5 will be studied using the Two-Modulator Generalized Ellipsometry Microscope (2-MGEM) and traditional polarized optical microscopy. This research will elucidate the

potential orientation of filler particles or binder phases and compare the results from the different grades. This analysis can help extend the understanding of microcracking that occurs during the irradiation of nuclear graphite. In general, nuclear graphite models assume that graphite is a monolithic material composed of a single phase. However, the ellipsometry results will help reveal the local anisotropy of the selected grades and show any preferential alignment of the binder or filler particles.

6. NEUTRON IRRADAITED AND OXIDIZED MICROSTRUCTURE LIBRARY

This part of the library will characterize the effects of neutron irradiation and oxidation using advanced characterization techniques. The objectives of this research include the following:

- Provide information on the microstructure of neutron irradiated graphite. This part of the library will document some of the irradiation effects on the microstructure in graphite at multiple irradiation or oxidation temperatures.
- Identify the mechanisms of irradiation dimensional change at different temperatures.
- Generate quantitative data on the defect cluster size and configuration of defects in graphite caused by either irradiation or oxidation.
- Characterize and estimate the pore size distribution contained in oxidized graphite caused by acute and uniform oxidation.

Some of the research conducted in this project thrust will focus on characterizing certain aspects of graphite that could be used to monitor the health of a nuclear graphite core.

6.1 MICROSTRUCTURAL CHARACTERIZATION DATA OF AS RECEIVED IG-110, 2114 AND ETU-10 GRAPHITE GRADES AND OXIDATION CHARACTERIZATION DATA OF IG-110

This part of the research was published in the journal article “Microstructural characterization data of as received IG-110, 2114 and ETU-10 nuclear graphite grades and oxidation characterization data of IG-110” [56] and can be found online as an open-access publication. This paper covers some characterization of the as-received microstructure of IG-110, 2114, and ETU-10 as well as the oxidized microstructure of IG-110. The data of this paper is available on the following online repository: https://data.mendeley.com/datasets/c4sj6yctkd.

6.1.1 FIB-SEM Tomography Characterization Of Neutron Induce Densification Of Quinoline Insoluble Particles

The binder phase of nuclear graphite contains some degree of QI particles. This study is focused on characterizing QI particles in graphite using FIB-SEM tomography. The primary objective is to examine the 3D structure of the particles of as-received material and determine the presence of any internal cracks. Then, neutron-irradiated samples will be characterized similarly to observe the crack morphological changes induced by neutron irradiation. Examples of the preliminary FIB-SEM tomography characterization and segmented 3D model of an unirradiated QI particle are shown in Figure 22.

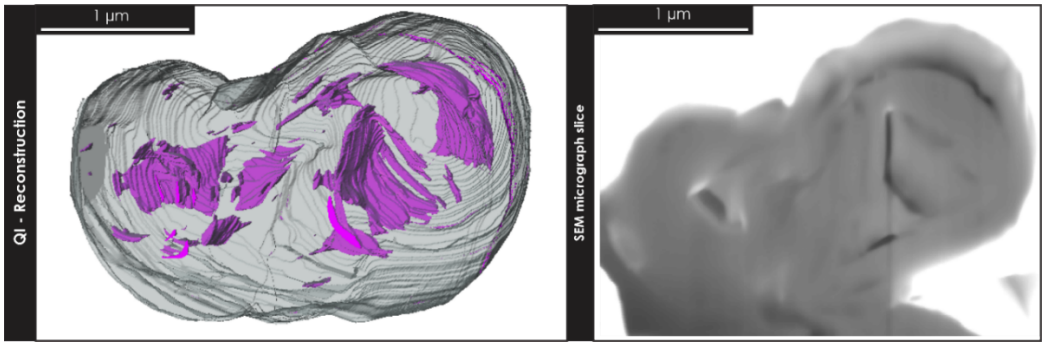

Figure 22. Reconstruction of a QI particle using FIB-SEM tomography and SEM micrograph that shows the cross section of the QI particle.

The external surface of this QI particle is shown in Figure 23. These SEM micrographs show that the QI particle can have complex shapes and can be formed by multiple merged particles.

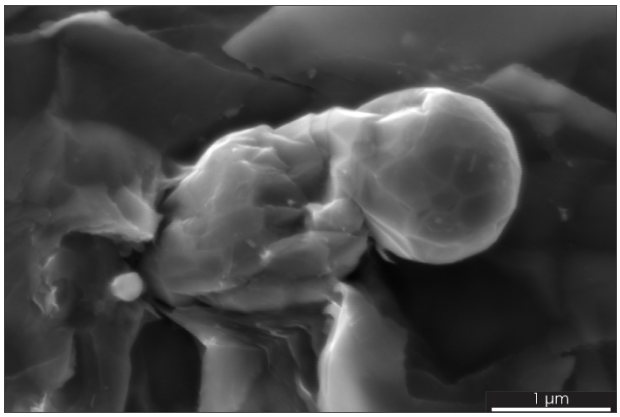

Figure 23. External surface of QI particle. These micrographs show the complex external morphology of QI particles.

QI particles might be highly susceptible to neutron and electron irradiation; therefore, they might be used as a forensic fingerprint of the damage generated by neutron irradiation. This project aims to determine whether QI particles might be used as indicators of the neutron induced damage in nuclear graphite.

6.1.2 Accident Conditions via XCT and Synchrotron XCT

Part of the assessment of oxidation on graphite might involve the examination of pore size and structure. Oxidation in nuclear graphite can occur during the normal operation of a nuclear power plant or as a result of accidental air ingress into the reactor core. Despite efforts to minimize oxidation by carefully controlling coolant chemistry, trace impurities may still exist. The gradual, long-term oxidation in nuclear graphite is called chronic oxidation. By contrast, the rapid reaction of large amounts of oxidation species with graphite components in a short period is known as *acute oxidation*.

This project focuses on conducting in situ oxidation experiments combined with synchrotron XCT to characterize the effects of oxidation on IG-110, PCEA, and NBG-18 graphite. The experimental setup used for these experiments is illustrated in Figure 24.

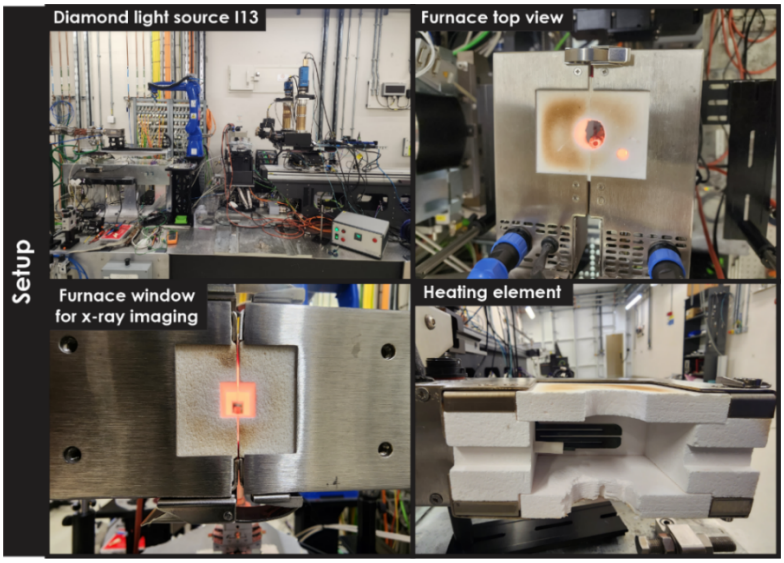

Figure 24. Diamond light source I13, furnace, and setup used for synchrotron XCT characterization. The images include the furnace top view that shows some holes that allow air access, the windows that allow the passage of the x-rays, and the heating elements used for the experiments.

Figure 25 presents selected images from the oxidation experiment conducted on IG-110 graphite. The graphite surface is progressively removed layer by layer at the specimen's edge, indicating localized acute oxidation behavior. The oxidation process also generates pores within the graphite and reduces density near the sample's edge, depicted as brighter regions. These findings contribute to understanding the extent of damage and microstructural changes associated with acute oxidation in modern nuclear-grade graphite. Additional analyses are underway to calculate parameters such as pore size distribution and porosity profiles, further elucidating the damage caused by acute oxidation. Some of these results will also help clarify the effectiveness of thermal treatments used for selective carbon-14 removal [57].

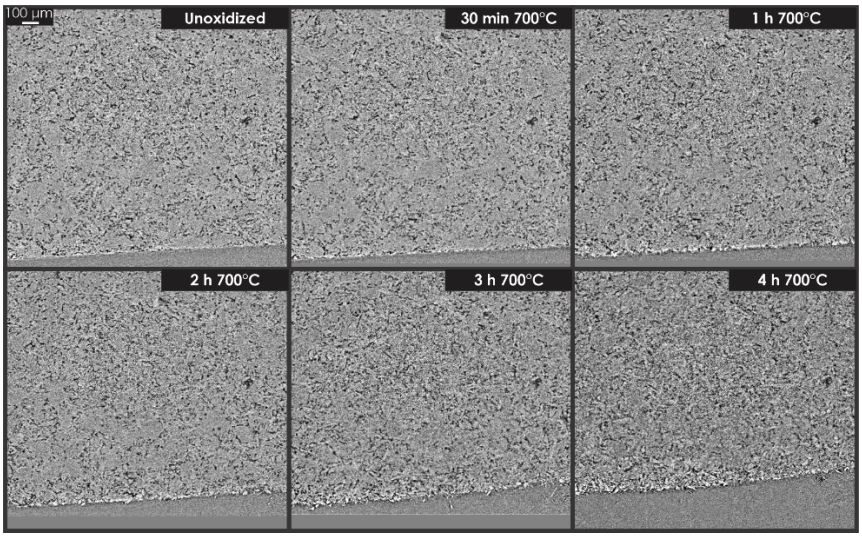

Figure 25. Synchrotron XCT slices of IG-110. The images show the deterioration of the microstructure produced by chronic oxidation

6.1.3 Characterization of Air-Oxidized Microstructure of Neutron-Irradiated ETU-10 Specimens

Some of the damage effects on graphite can be tracked via the size and shape of pores because porosity plays an essential role in the mechanical property degradation of nuclear graphite. Nuclear graphite can be subjected to oxidation during the regular operation of a nuclear power plant or during an accident that causes air ingress to the reactor core. Although the chemistry of the coolant during normal operating conditions can be controlled, small quantities of impurities will be present in the coolant mixtures. This type of oxidation in nuclear graphite is normally described as *chronic oxidation*. The entry of oxidant species under an accidental ingress of air to the graphite core would induce what is referred to as *acute oxidation*. Limited research has been conducted on the effects of oxidation on nuclear graphite's microstructure or elastic properties. This project will analyze the effects of oxidation on ETU-10 neutron-irradiated specimens' microstructure via XCT. This data will help determine the extent of damage generated by chronic oxidation or during the accidental ingress of air to a reactor core. This research will elucidate the combined effects of oxidation and neutron irradiation. Neutron irradiation might accelerate the rate of oxidation in graphite because of the defects introduced in the graphite crystal lattice and the creation of nanopores. In other words, introducing defects might act as additional active sites generally absent in as received graphite. This project is at an early stage. Samples are being prepared to start the characterization stage. This research is being supported by a Nuclear Science User Facilities Rapid Turnaround Experiment proposal.

7. NON-GRAPHITE CARBON-BASED LIBRARY OF MICROSTRUES FOR NUCLEAR APPLICATIONS

7.1 NEUTRON IRRADIATION EFFECTS IN GLASSY CARBON

Glassy carbon is an allotrope of carbon formed by sp^2 bonding considered once for multiple nuclear applications owing to its chemical inertness and its desirable mechanical properties. The neutron irradiation effects in glassy carbon were investigated by combining dimensional analysis, scanning transmission electron microscopy, and Raman spectroscopy to understand the link between dimensional changes and atomic structure. Glassy carbon is formed by planar 2D bonded sp^2 structures that are usually absent in amorphous carbons. The planar carbon domains resemble the graphitized content of other materials, but these domains contain many defects normally absent from graphitic materials. Perhaps the most similar carbon material to glassy carbon is graphite. As glassy carbon, graphite is formed by sp^2 hybridized aromatic carbon. However, glassy carbon cannot be graphitized by conventional heat treatments. The irradiation behavior of glassy carbon is being investigated because of its similarities to graphite and other graphitic materials.

All the irradiated samples showed a significant shrinkage at the different temperature conditions and a significant irradiation–temperature dependence, as shown in Figure 26. The historical data in Figure 26 suggest that glassy carbon might not exhibit a turnaround or require larger neutron doses than graphite or nuclear-grade pyrolytic carbons to reach turnaround.

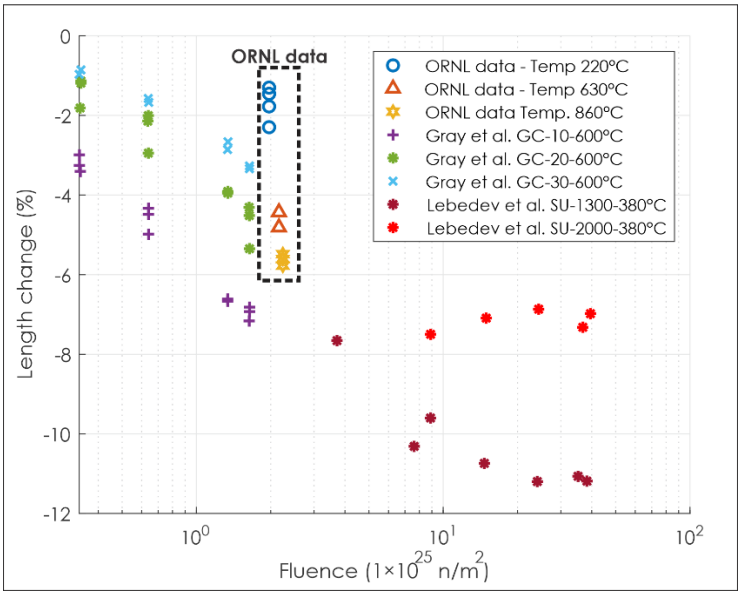

Figure 26. Neutron-induced dimensional change in glassy carbon. Data from ORNL and historical data.

The micrographs included in Figure 27 demonstrate that the process of neutron-induced densification of glassy carbon depends on the irradiation temperature. At low temperatures, the carbon strands that form the glassy carbon appear amorphized, whereas at high temperatures, the strands appear to restructure, closing the pores.

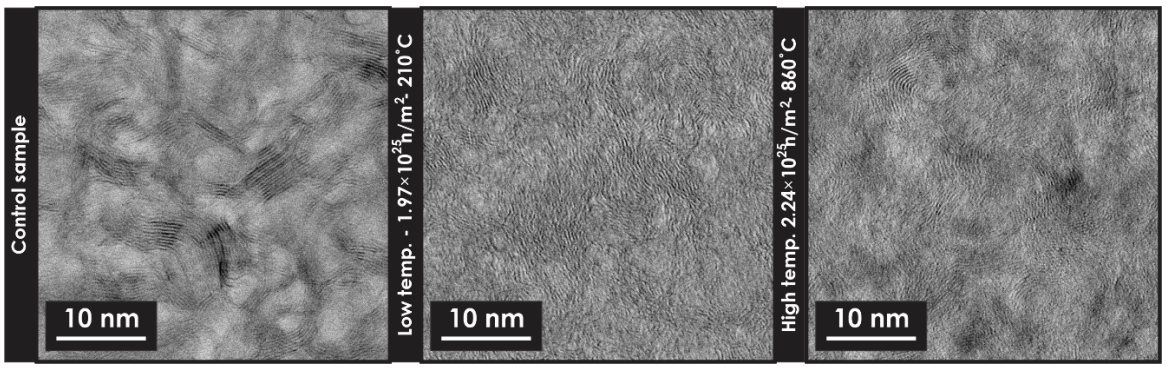

Figure 27. Scanning electron microscopy micrographs of unirradiated and neutron-irradiated glassy carbon.

Figure 28 shows two distinctive postirradiation Raman spectrum behaviors. The change produced by the lowest irradiation temperature condition at 220°C had a significant difference in Raman shift, confirming the partial amorphization of the material. The higher irradiation temperatures above 630°C produced an increase of sp^2 sites or, in other words, an increase in G peak intensity values. These and other results included in this research are being compared with graphite and other common graphitic materials used in the nuclear industry. A better insight into the irradiation effects in glassy carbon will contribute to the understanding of neutron-induced damage in the nongraphitizable phases of graphitic materials.

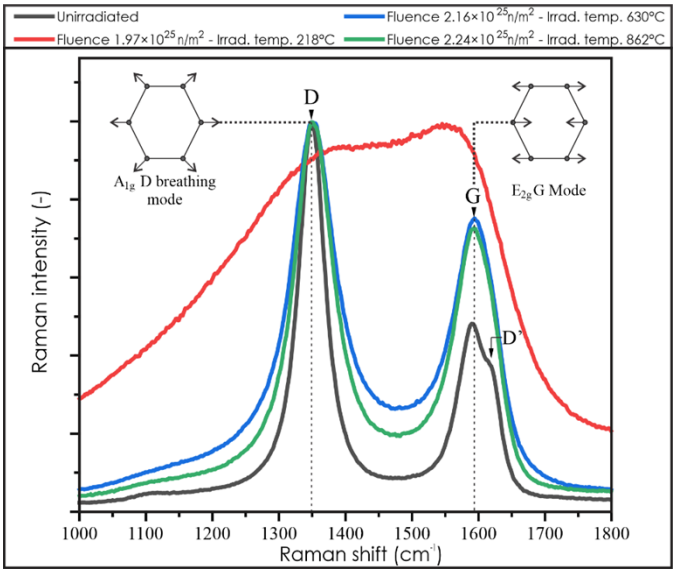

Figure 28. Raman spectroscopy results of as-received and neutron-irradiated specimens of glassy carbon.

7.2 MICROSTRUCTURAL CHARACTERIZATION OF PYROLYTIC CARBON

Pyrolytic carbons form part of the tri-structural isotropic (TRISO) particle fuels. Silicon carbide composites interface with and are proposed as a coating for nuclear graphite. This part of the library will focus on characterizing these materials to understand the irradiation effects in graphite and its suitability as a protective layer for nuclear graphite.

8. SUMMARY

This project is developing a comprehensive library of data that describe some of graphite's most important characteristics and microstructures. This project's strategy includes aid with the design, modeling, aging management, and decommissioning of graphite components. Moreover, these efforts are dedicated to understanding the uncertainty caused by microstructural variations in graphite. This variability causes mechanical property differences that must be accounted for in the design and safety cases. Improving the characterization and understanding of irradiation effects in graphite reduction will help develop appropriate measures to account for variations in graphite. The research focuses on the baseline characterization of unirradiated material, a guide to techniques commonly used to characterize graphite, research on defects generated by oxidation or irradiation, and an investigation of some materials similar to graphite commonly used in the nuclear industry.

Another core element of this research is to provide guidance outlining a protocol that assesses the consistency of grades and graphite components. All aspects of this report also outline some preliminary results that will enhance the knowledge and understanding of graphite's microstructure and aging mechanisms. The current and future efforts of the library of microstructures is shown in the Gantt chart in Figure 29.

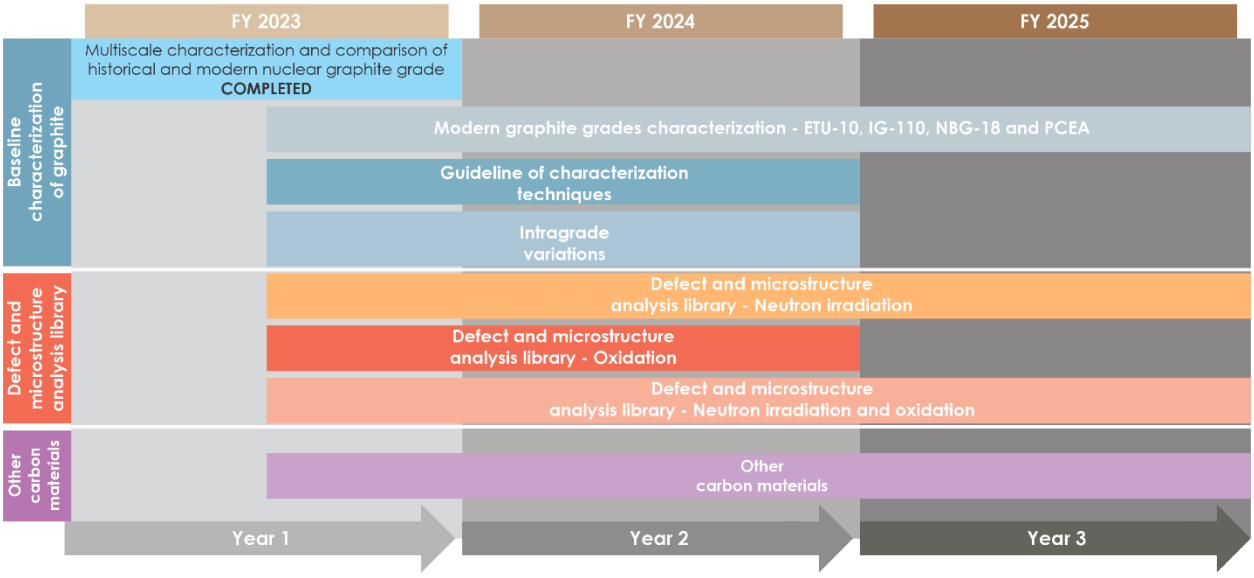

Figure 29. Gantt chart of current progress and future efforts of the library of microstructure for nuclear graphite.

This report summarizes the development of characterization techniques, current state of the microstructural data and other related activities that support the US nuclear graphite programs. A summary of the characterization performed on the historical and modern grades is given in Table 9. This table lists the basic information of the grades and techniques used for each grade. The column that indicates the progress described in Table 9 refers to the competition of the overall task. However, five grades were selected (IG-110, NBG-18, 2114, PCEA and ETU-10) for further investigation because of their importance and relevance to the US nuclear graphite programs. These grades will be further studied to further elucidate the characteristics, oxidation effects, and irradiation response on these grades. Some of the proposed characterization techniques for these grades are given in Table 10. Some of the activities related to the characterization of oxidized and neutron-irradiated samples are listed in Table 11. These activities will form part of the library dedicated to environmental effects in nuclear graphite.

Table 9. List of current status surveyed specimens, techniques and description of selected graphite grades

Graphite grade	Coke source	Type	Nominal grain size (μm)	Manufacturer	Application/ Reactor	Analysis techniques	Current progress
ZXF-5Q	Not provided	Microfine	1	POCO	Gen IV reactors	He, MP, FBT, SEM, TEM	Completed
AXF-5Q	Not provided	Ultrafine	5	POCO	Gen IV reactors	He, MP, POM, SEM, TEM, XCT	Completed
TM	Not provided	Superfine	10	POCO	Gen IV reactors	He, MP, POM, SEM, XCT	Completed
IG-430	Pitch coke	Superfine	10	Toyo Tanso	Gen IV reactors	POM, SEM, XCT	Completed
2114	Nonpetroleum coke	Superfine	13	Mersen	Gen IV reactors	He, MP, POM, SEM, TEM, XCT	**Incomplete**
2020	Petroleum	Superfine	15	Mersen	Gen IV reactors	POM	Completed
ETU-10	Coal-tar pitch	Superfine	15	Ibiden	Gen IV reactors	He, MP, POM, SEM, TEM, XCT	**Incomplete**
IG-110	Petroleum coke	Superfine	20	Toyo Tanso	Gen IV reactors	He, MP, POM, SEM, TEM, XCT	**Incomplete**
G347A	Coal	Superfine	50	Tokai Carbon Co., Ltd.	Gen IV reactors	POM, XCT	Completed
NBG-25	Petroleum	Fine	60	SGL, Carbon	Gen IV reactors	He, MP, POM	Completed
Gilsocarbon	Gilsonite	Medium-fine	500	AGL, Union Carbide	AGRs	POM, SEM, TEM, XCT	Completed
H-451	Petroleum	Medium-fine	500	SGL, Carbon	HTGR	POM	Completed
HLM	Petroleum	Medium-fine	800	SGL, Carbon	Reflector	POM, SEM, TEM, XCT	Completed
NBG-17	Pitch	Medium-fine	800	SGL, Carbon	Gen IV reactors	He, MP, POM, SEM, TEM, XCT	Completed
PCEA	Petroleum	Medium-fine	800	Graftech	Gen IV reactors	He, MP, POM, SEM, TEM, XCT	**Incomplete**
PGA	Petroleum	Medium-fine	800	British Acheson Electrodes, Ltd.	Magnox reactors	POM	Completed
NBG-18	Pitch	Medium-coarse	1600	SGL, Carbon	Gen IV reactors	He, MP, POM, SEM, TEM, XCT	**Incomplete**
AGX	Petroleum	Coarse	6350	National Carbon Co.	Electrode	POM	Completed
AGOT*	Variable	Variable	Variable	National Carbon Co.	Chicago and Hanford piles	POM	Completed
TSX*	Petroleum	Unknown	Unknown	National Carbon Co.	Hanford reactor (N Reactor)	POM	Completed
HG**	Petroleum	Unknown	Unknown	Unknown	NRU thermal column	SEM, TEM	Completed
HOPG	—	—	—	—	—	EBSD, SEM	Completed

Note: EBSD = electron backscatter diffraction, FBT = FIB-SEM tomography, He = helium pycnometry, MP = mercury porosimetry, POM = polarized optical microscopy, SEM = scanning electron microscopy, XCT = x-ray computed tomography.
*This graphite has several incarnations or versions, so the grain size is variable
**HG graphite was part of the NRU thermal column.

Table 10. Selected graphite grades for advanced characterization

Graphite grade	Coke source	Type	Grain size (μm)	Manufacturer	Techniques
2114	Nonpetroleum coke	Superfine	13	Mersen	Ellipsometry, Serial sectioning with optical microscopy, PFIB-SEM tomography
ETU-10	Coal-tar pitch	Superfine	15	Ibiden	
IG-110	Petroleum coke	Superfine	20	Toyo Tanso	
PCEA	Petroleum	Medium-fine	800	Graftech	
NBG-18	Pitch	Medium-coarse	1,600	SGL, Carbon	

Table 11. Characterization matrix for oxidized, neutron-irradiated and oxidized-neutron-irradiated graphite specimens

Graphite grade	Manufacturer	Type	Type of sample	Techniques
2114	Mersen	Superfine	Neutron irradiated	TEM, FIB-SEM tomography
ETU-10	Ibiden	Superfine	Neutron irradiated	TEM, optical microscopy
			Neutron irradiated and oxidized	XCT
IG-110	Toyo Tanso	Superfine	Uniform and acute oxidation	XCT
			Neutron irradiated	TEM
PCEA	Graftech	Medium-fine	Uniform and acute oxidation	XCT
			Neutron irradiated	TEM, FIB-SEM tomography
NBG-18	SGL, Carbon	Medium-coarse	Uniform and acute oxidation	XCT
			Neutron irradiated	TEM

9. REFERENCES

[1] X.-w. Zhou, Y.-p. Tang, Z.-m. Lu, J. Zhang, B. Liu, Nuclear graphite for high temperature gas-cooled reactors, New Carbon Materials 32(3) (2017) 193-204.

[2] J.J. Lee, J.D. Arregui-Mena, C.I. Contescu, T.D. Burchell, Y. Katoh, S.K. Loyalka, Protection of graphite from salt and gas permeation in molten salt reactors, Journal of Nuclear Materials 534 (2020) 152119.

[3] R.E. Nightingale, Nuclear Graphite, Academic Press1962.

[4] J.D. Arregui-Mena, R.N. Worth, G. Hall, P.D. Edmondson, A.B. Giorla, T.D. Burchell, A Review of Finite Element Method Models for Nuclear Graphite Applications, Archives of Computational Methods in Engineering 27(1) (2020) 331-350.

[5] J.D. Arregui-Mena, D.V. Griffiths, R.N. Worth, C.E. Torrence, A. Selby, C. Contescu, N. Gallego, P.D. Edmondson, P.M. Mummery, L. Margetts, Using porous random fields to predict the elastic modulus of unoxidized and oxidized superfine graphite, Materials & Design 220 (2022) 110840.

[6] W.E. Windes, T.D. Burchell, M. Davenport, The advanced reactor technologies (art) graphite R&D program, Nuclear Engineering and Design 362 (2020) 110586.

[7] M. Inagaki, F. Kang, M. Toyoda, H. Konno, 17. Isotropic High-Density Graphite and Nuclear Applications, Advanced Materials Science and Engineering of Carbon, Elsevier2014.

[8] J.D. Arregui-Mena, P.D. Edmondson, A.A. Campbell, Y. Katoh, Site specific, high-resolution characterisation of porosity in graphite using FIB-SEM tomography, Journal of Nuclear Materials 511 (2018) 164-173.

[9] P. Yan, J.F.B. Delannay, A. Tzelepi, A micromechanistic crystal plasticity model for graphite in: P.E.J. Flewitt, A.J. Wickham (Eds.) 4th EDF Energy Nuclear Graphite Symposium, EMAS, 2014.

[10] A.L. Sutton, V.C. Howard, The role of porosity in the accommodation of thermal expansion in graphite, Journal of Nuclear Materials 7(1) (1962) 58-71.

[11] H.M. Freeman, A.N. Jones, M.B. Ward, F.S. Hage, N. Tzelepi, Q.M. Ramasse, A.J. Scott, R.M.D. Brydson, On the nature of cracks and voids in nuclear graphite, Carbon 103 (2016) 45-55.

[12] P.J. Hacker, G.B. Neighbour, B. McEnaney, The coefficient of thermal expansion of nuclear graphite with increasing thermal oxidation, Journal of Physics D, Applied Physics 33(8) (2000) 991-998.

[13] ASTM, D7219-19 - Standard specification for Isotropic and near-isotropic nuclear graphite, ASTM, ASTM, 2019.

[14] T.D. Burchell, A microstructurally based fracture model for polygranular graphites, Carbon 34(3) (1996) 297-316.

[15] C.I. Contescu, T.D. Burchell, Characterization of Porosity Development in Oxidized Graphite using Automated Image Analysis Techniques, ORNL, Oak Ridge, TN, 2009.

[16] J. Kane, C. Karthik, D.P. Butt, W.E. Windes, R. Ubic, Microstructural characterization and pore structure analysis of nuclear graphite, Journal of Nuclear Materials 415(2) (2011) 189-197.

[17] P. Wang, C.I. Contescu, S. Yu, T.D. Burchell, Pore structure development in oxidized IG-110 nuclear graphite, Journal of Nuclear Materials 430(1) (2012) 229-238.

[18] C.I. Contescu, T. Guldan, P. Wang, T.D. Burchell, The effect of microstructure on air oxidation resistance of nuclear graphite, Carbon 50(9) (2012) 3354-3366.

[19] T. Manuwong, G.D. Kipling, G.B. Neighbour, Quantitative Microstructure Characterisation of Advanced Carbon Using Image Analysis, Conference on Modelling and Measuring Reactor Core Graphite Properties and Performance, The British Carbon Group, Birmingham, 2013.

[20] K. Takizawa, T. Fukuda, A. Kondo, Y. Katoh, G.E. Jellison, Microstructural Analysis of Nuclear Grade Graphite Materials, Ceramic Materials for Energy Applications II2013, pp. 133-144.

[21] M. M.P., A. Tzelepi, Applications of optical microscopy to study changes in grahite microstructure, in: P.E.J.F.a.A.J. Wickham (Ed.) The 4th EDF Energy Nuclear Graphite Symposium - Engineering Challenges Associated with the LIfe of Graphite Reactors Cores, EMAS, Nottingham, Uk, 2015.

[22] Q. Huang, H. Tang, Porosity analysis of superfine-grain graphite IG-110 and ultrafine-grain graphite T220, Materials Science and Technology 35(8) (2019) 962-968.
[23] H. Badenhorst, Graphite oxidation and SEM as a tool for microstructural investigation, Transactions of the Royal Society of South Africa 72 (2017) 294 - 300.
[24] S.M. Barhli, L. Saucedo-Mora, M.S.L. Jordan, A.F. Cinar, C. Reinhard, M. Mostafavi, T.J. Marrow, Synchrotron X-ray characterization of crack strain fields in polygranular graphite, Carbon 124 (2017) 357-371.
[25] W. Bodel, P. Martinuzzi, B. Davies, A. Steer, T. Lowe, P. Mummery, Mimicking irradiation-induced cracking of nuclear graphite using bromine intercalation, Scripta Materialia 199 (2021) 113889.
[26] J.D. Arregui-Mena, T. Koyanagi, E. Cakmak, C.M. Petrie, W.-J. Kim, D. Kim, C.P. Deck, C. Sauder, J. Braun, Y. Katoh, Qualitative and quantitative analysis of neutron irradiation effects in SiC/SiC composites using X-ray computed tomography, Composites Part B: Engineering 238 (2022) 109896.
[27] H. Wang, T. Koyanagi, D.J. Arregui-Mena, Y. Katoh, Anisotropic thermal diffusivity and conductivity in SiC/SiC tubes studied by infrared imaging and X-ray computed tomography, Ceramics International 48(15) (2022) 21717-21727.
[28] J.D. Arregui-Mena, R.L. Seibert, T.J. Gerczak, Characterization of PyC/SiC Interfaces with FIB-SEM Tomography, Journal of Nuclear Materials 545 (2021) 152736.
[29] J.D. Arregui-Mena, C.I. Contescu, A.A. Campbell, P.D. Edmondson, N.C. Gallego, Q.B. Smith, K. Takizawa, Y. Katoh, Nitrogen adsorption data, FIB-SEM tomography and TEM micrographs of neutron-irradiated superfine grain graphite, Data in Brief 21 (2018) 2643-2650.
[30] J. Koike, D.F. Pedraza, Dimensional changes in highly oriented pyrolytic graphite due to electron-irradiation, Journal of Materials Research 9(7) (1994) 1899-1907.
[31] Y.I. Shtrombakh, B.A. Gurovich, P.A. Platonov, V.M. Alekseev, Radiation damage of graphite and carbon-graphite materials, Journal of Nuclear Materials 225 (1995) 273-301.
[32] A.P. Burden, J.L. Hutchison, In situ fullerene formation—The evidence presented, Carbon 36(7) (1998) 1167-1173.
[33] K. Wen, J. Marrow, B. Marsden, Microcracks in nuclear graphite and highly oriented pyrolytic graphite (HOPG), Journal of Nuclear Materials 381(1) (2008) 199-203.
[34] C. Karthik, J. Kane, D.P. Butt, W.E. Windes, R. Ubic, In situ transmission electron microscopy of electron-beam induced damage process in nuclear grade graphite, Journal of Nuclear Materials 412(3) (2011) 321-326.
[35] C. Karthik, J. Kane, D.P. Butt, W.E. Windes, R. Ubic, Microstructural Characterization of Next Generation Nuclear Graphites, Microscopy and Microanalysis 18(2) (2012) 272-278.
[36] A.A. Campbell, K.B. Campbell, G.S. Was, Anisotropy analysis of ultra-fine grain graphite and pyrolytic carbon, Carbon 60 (2013) 410-420.
[37] B.E. Mironov, H.M. Freeman, A.P. Brown, F.S. Hage, A.J. Scott, A.V.K. Westwood, J.P. Da Costa, P. Weisbecker, R.M.D. Brydson, Electron irradiation of nuclear graphite studied by transmission electron microscopy and electron energy loss spectroscopy, Carbon 83 (2015) 106-117.
[38] C. Karthik, J. Kane, D.P. Butt, W.E. Windes, R. Ubic, Neutron irradiation induced microstructural changes in NBG-18 and IG-110 nuclear graphites, Carbon 86 (2015) 124-131.
[39] R. Krishna, A.N. Jones, L. McDermott, B.J. Marsden, Neutron irradiation damage of nuclear graphite studied by high-resolution transmission electron microscopy and Raman spectroscopy, Journal of Nuclear Materials 467 (2015) 557-565.
[40] H.M. Freeman, A.J. Scott, R.M.D. Brydson, Thermal annealing of nuclear graphite during in-situ electron irradiation, Carbon 115 (2017) 659-664.
[41] B. März, K. Jolley, T.J. Marrow, Z. Zhou, M. Heggie, R. Smith, H. Wu, Mesoscopic structure features in synthetic graphite, Materials & Design 142 (2018) 268-278.
[42] D. Liu, D. Cherns, Nano-cracks in a synthetic graphite composite for nuclear applications, Philosophical Magazine 98(14) (2018) 1272-1283.
[43] S. Johns, T. Poulsen, J.J. Kane, W.E. Windes, R. Ubic, C. Karthik, Formation of carbon nanostructures in nuclear graphite under high-temperature in situ electron-irradiation, Carbon 143 (2019) 908-914.

[44] S. Johns, L. He, K. Bustillo, W.E. Windes, R. Ubic, C. Karthik, Fullerene-like defects in high-temperature neutron-irradiated nuclear graphite, Carbon 166 (2020) 113-122.
[45] J.D. Arregui-Mena, D.A. Cullen, R.N. Worth, S.V. Venkatakrishnan, M.S.L. Jordan, M. Ward, C.M. Parish, N. Gallego, Y. Katoh, P.D. Edmondson, N. Tzelepi, Electron tomography of unirradiated and irradiated nuclear graphite, Journal of Nuclear Materials 545 (2021) 152649.
[46] D. Liu, D. Cherns, S. Johns, Y. Zhou, J. Liu, W.-Y. Chen, I. Griffiths, C. Karthik, M. Li, M. Kuball, J. Kane, W. Windes, A macro-scale ruck and tuck mechanism for deformation in ion-irradiated polycrystalline graphite, Carbon 173 (2021) 215-231.
[47] J.D. Arregui-Mena, R.N. Worth, W. Bodel, B. März, W. Li, A.A. Campbell, E. Cakmak, N. Gallego, C. Contescu, P.D. Edmondson, Multiscale characterization and comparison of historical and modern nuclear graphite grades, Materials Characterization 190 (2022) 112047.
[48] J.D. Arregui-Mena, R.N. Worth, W. Bodel, B. März, W. Li, A. Selby, A.A. Campbell, C. Contescu, P.D. Edmondson, N. Gallego, SEM and TEM data of nuclear graphite and glassy carbon microstructures, Data in Brief 46 (2023) 108808.
[49] J.D. Arregui-Mena, P.D. Edmondson, D. Cullen, S. Levine, C. Contescu, Y. Katoh, N. Gallego, Microstructural characterization of the CGB graphite grade from the molten salt reactor experiment, Journal of Nuclear Materials 582 (2023) 154421.
[50] J.D. Arregui-Mena, W. Bodel, R.N. Worth, L. Margetts, P.M. Mummery, Spatial variability in the mechanical properties of Gilsocarbon, Carbon 110 (2016) 497-517.
[51] J.D. Arregui-Mena, P.D. Edmondson, L. Margetts, D.V. Griffiths, W.E. Windes, M. Carroll, P.M. Mummery, Characterisation of the spatial variability of material properties of Gilsocarbon and NBG-18 using random fields, Journal of Nuclear Materials 511 (2018) 91-108.
[52] J.D. Arregui-Mena, L. Margetts, P.M. Mummery, Practical Application of the Stochastic Finite Element Method, Archives of Computational Methods in Engineering 23(1) (2016) 171-190.
[53] J.D. Arregui-Mena, L. Margetts, D.V. Griffiths, L. Lever, G. Hall, P.M. Mummery, Spatial variability in the coefficient of thermal expansion induces pre-service stresses in computer models of virgin Gilsocarbon bricks, Journal of Nuclear Materials 465 (2015) 793-804.
[54] T.J. Gerczak, A.A. Campbell, G.W. Helmreich, G.E. Jellison, J.D. Hunn, Texture analysis of AGR program matrix materials, Nuclear Engineering and Design 398 (2022) 111965.
[55] C.I. Contescu, J.D. Arregui-Mena, A.A. Campbell, P.D. Edmondson, N.C. Gallego, K. Takizawa, Y. Katoh, Development of mesopores in superfine grain graphite neutron-irradiated at high fluence, Carbon 141 (2019) 663-675.
[56] J.D. Arregui-Mena, D.V. Griffiths, R.N. Worth, C.E. Torrence, A. Selby, C. Contescu, N. Gallego, P.D. Edmondson, P.M. Mummery, L. Margetts, Microstructural characterization data of as received IG-110, 2114 and ETU-10 nuclear graphite grades and oxidation characterization data of IG-110, Data in Brief 44 (2022) 108535.
[57] R.N. Worth, A. Theodosiou, W. Bodel, J.D. Arregui-Mena, A.J. Wickham, A.N. Jones, P.M. Mummery, The distribution and selective decontamination of carbon-14 from nuclear graphite, Journal of Nuclear Materials 556 (2021) 153167.